Clim. Past, 18, 2117–2142, 2022
https://doi.org/10.5194/cp-18-2117-2022
© Author(s) 2022. This work is distributed under
the Creative Commons Attribution 4.0 License.

Climate of the Past
Open Access

Shallow marine carbonates as recorders of orbitally induced past climate changes – example from the Oxfordian of the Swiss Jura Mountains

André Strasser[1]

[1]Department of Geosciences, University of Fribourg, Fribourg, 1700, Switzerland
Invited contribution by André Strasser, recipient of the EGU Jean Baptiste Lamarck Medal 2021.

Correspondence: André Strasser (andreas.strasser@unifr.ch)

Received: 18 March 2022 – Discussion started: 25 March 2022
Revised: 4 August 2022 – Accepted: 9 August 2022 – Published: 14 September 2022

Abstract. Today and in the geologic past, climate changes greatly affect and have affected Earth surface processes. While the climatic parameters today can be measured with high precision, they have to be interpreted from the sedimentary record for ancient times. This review is based on the detailed analysis of stratigraphic sections of Oxfordian (Late Jurassic) age, with the aim to reconstruct and discuss the climate changes that controlled the sedimentation on the shallow marine carbonate platform that today is represented in the Swiss Jura Mountains. The sediments formed under subtropical conditions in which carbonate-producing organisms proliferated, and ooids and oncoids were common. The sections are composed of hierarchically stacked elementary, small-scale, and medium-scale depositional sequences wherein facies changes imply deepening–shallowing trends. The major sequence boundaries Ox 6, Ox 7, and Ox 8 can be correlated with those of other European basins and place the studied sections in a broader framework. The chronostratigraphic tie points imply that the medium- and small-scale sequences formed in tune with the orbital eccentricity cycles of 405 and 100 kyr, respectively, and the elementary sequences with the precession cycle of 20 kyr. Orbitally controlled insolation changes at the top of the atmosphere translated into climate changes: low insolation generally resulted in low amplitudes of sea level fluctuations at the 20 kyr frequency and in a cool and humid climate at the palaeolatitude of the Jura platform. Terrigenous material was eroded from the hinterland and distributed over the platform. High insolation led to sea level rise, as well as to warm and semiarid to arid conditions in which coral reefs could grow. However, nutrient input favoured growth of microbialites that encrusted the corals. The reconstruction of high-frequency sea level fluctuations based on facies analysis compares well with the curve of insolation changes calculated for the past 550 kyr. It is therefore assumed that the sea level fluctuations were mainly due to thermal expansion and retraction of ocean surface water. Two models are presented that explain the formation of elementary sequences: one for low and one for high insolation. Despite the important lateral facies variations typical of a shallow marine platform, and despite the uncertainties in the reconstruction of sea level changes, this study demonstrates the potential of carbonate ecosystems to record past climate changes at a time resolution of 20 000 years. Relatively short time windows can thus be opened in the deep geologic past, and processes and products there can be compared with those of the Holocene and the Anthropocene. For example, it appears that today's anthropogenically induced sea level rise is more than 10 times faster than the fastest rise reconstructed for the Oxfordian.

1 Introduction

In today's world of global climate change and its impact on *Homo sapiens*, research into past climate variability as recorded in sediments is becoming particularly interesting. Rapid and profound climate-induced changes in palaeoecosystems can thus be documented and may serve as examples of changes we may experience in the near future.

Orbital cycles (Milankovitch cycles) are an important factor steering global climate as they control the amount of so-

lar energy received by the Earth. The quasi-periodicities of these cycles (precession, obliquity, short and long eccentricity) have been calculated from today back to the Precambrian (e.g. Berger et al., 1992; Laskar et al., 2011; Hinnov, 2018). They are used to calibrate geological timescales (e.g. Gradstein et al., 2020) and to reconstruct past climate changes with a high time resolution. At the Equator, the daily insolation fluctuates around 400 W m^{-2}, with the precession cycle modulated by the eccentricity cycles. At higher latitudes the insolation values are higher, with higher amplitudes, and the obliquity signal is better expressed (Fig. 1). Today, the frequency peaks of precession are at 21 and 23 kyr, the obliquity at 41 kyr, the short eccentricity at 100 kyr, and the long eccentricity at 405 kyr. While the eccentricity cycles stay constant through time, precession and obliquity were shorter in the geological past (Berger et al., 1992; Hinnov, 2018). In the Oxfordian (Late Jurassic) considered here, the precession cycle had a value of about 20 kyr.

In deep-water sedimentary records, the effects of the orbital cycles on sedimentation have been well documented for many geological periods. For example, Amies et al. (2019) explained how sapropel formation in the Mediterranean basin reflects a northward migration of the monsoon rain belt over North Africa during the last interglacial, and this migration was controlled by the precession cycle (Lourens et al., 1996). Another example comes from the Valanginian and Hauterivian in the Vocontian basin analysed by Martinez (2018), where precession, obliquity, and the two eccentricity cycles are held responsible for the formation of repetitive, hemipelagic limestone–marl alternations and which help refining the duration of these two stages. In the Kimmeridge Clay Formation of the UK, Armstrong et al. (2016) documented the short and long eccentricity cycles that periodically induced extremely humid conditions leading to high burial of organic matter. In the Paleogene–Neogene Ebro Basin, Valero et al. (2014) described a 20 Myr lacustrine sedimentary record that formed in tune with the orbital eccentricity cycles.

In deep marine or deep lacustrine basins, there is a good chance that sedimentation was relatively continuous and interrupted only by tectonic pulses or gravitational flows. Sea level falls have an indirect influence by forcing progradation and thus an increase in turbidity currents and debris flows. On shallow platforms and ramps, however, minor sea level drops can lead to subaerial exposure and thus to hiatuses in the sedimentary record (e.g. Sadler, 1994; Strasser, 2015). Also, the depositional environment is much less homogenous than in deep-water settings: facies changes may occur over short (100 m scale) distances, creating facies mosaics (e.g. Rankey and Reeder, 2010). Nevertheless, shallow marine carbonates also have potential to record climate changes at a (geologically speaking) high time resolution.

Carbonate-producing marine organisms such as corals, calcareous algae, bivalves, gastropods, echinoderms, foraminifera, or serpulids are sensitive to water depth, water temperature, water energy, water chemistry, turbidity, nutrients, and substrate, which are all factors that are directly or indirectly controlled by climate. Carbonate particles such as ooids or oncoids commonly form under the influence of microbes, and calcifying microbes can build up stromatolites or thrombolites. The microbial communities again are dependent on multiple ecological factors and thus on climate.

Orbital cycles induce insolation changes at the top of the atmosphere, dependent on the latitude (Fig. 1). The translation of insolation changes into climate changes that ultimately influence the shallow marine carbonate platform or ramp is complex and passes through atmospheric and oceanic circulation (Fig. 2), which are themselves dependent on latitude, orography, and land–ocean distribution, as well as on the shape and position of the oceanic basins (e.g. Feng and Poulsen, 2014). Multiple feedback processes occur with different frequencies and amplitudes. For example, vegetation or ice cover will modify the albedo, or sea level change, ocean dynamics, and nutrient cycling may impact atmospheric CO_2 levels and water chemistry (e.g. Wallmann et al., 2016). This will finally result in the regional climate that influences the carbonate platform under investigation (air and water temperature, rainfall, wind, and seasonality). However, it also has to be considered that if the seasonal insolation change is below a certain threshold it may not induce a significant climate change and will not be recorded in the sedimentary system (Hinnov, 2018). In this paper, only subtropical carbonate systems are considered, and the following case study deals with such sediments. In fact, carbonates are produced in different "factories", from tropical to cool water and from shallow to deep (Flügel, 2004; Reijmer, 2021).

Sea level is an important factor that controls water depth. Water depth influences the growth of calcareous algae that use photosynthesis and of carbonate-producing organisms that contain light-dependent symbionts such as corals. Wave action in shallow water reworks the sediment and winnows out the mud fraction, while in deeper water carbonate mud can accumulate. The formation of ooid shoals is most efficient in a regime of tidal currents, which are strongest in shallow channels (e.g. Flügel, 2004; Reijmer, 2021). Sea level also controls accommodation, i.e. the potential to accumulate the sediment. Eustatic sea level changes were highly asymmetrical in icehouse worlds through slow buildup of polar ice caps and mountain glaciers, followed by rapid melting. The amplitudes were of the order of tens of metres (120 m during the last glacial–interglacial cycle; Shackleton, 1987). In greenhouse worlds such as the Late Jurassic (e.g. Sellwood and Valdes, 2008), the sea level changes were metre-scale only, caused by changes in ice volume of small polar ice caps and glaciers, thermally controlled volume changes in the ocean surface waters, density-controlled volume changes in deep ocean waters, and/or changes in the volume of fresh water sequestered on the continents (Schulz and Schäfer-

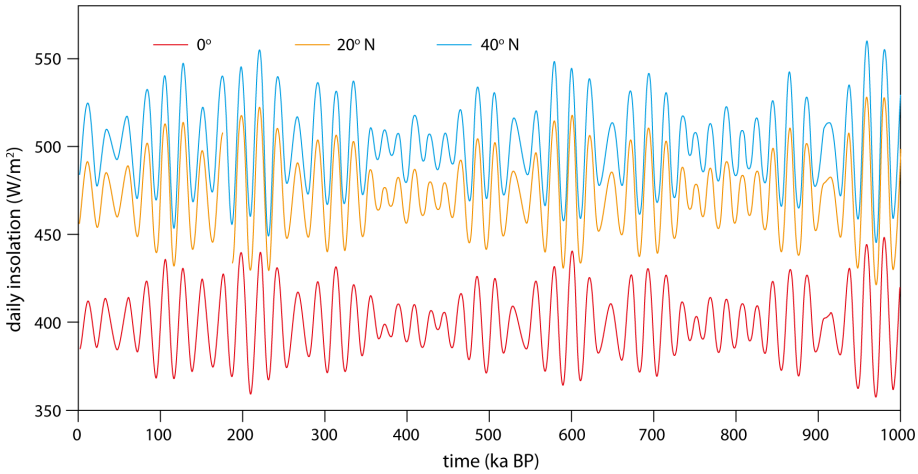

Figure 1. Mean daily insolation values for 21 June (northern summer solstice) at different latitudes, calculated for the last million years (modified from Hinnov, 2018).

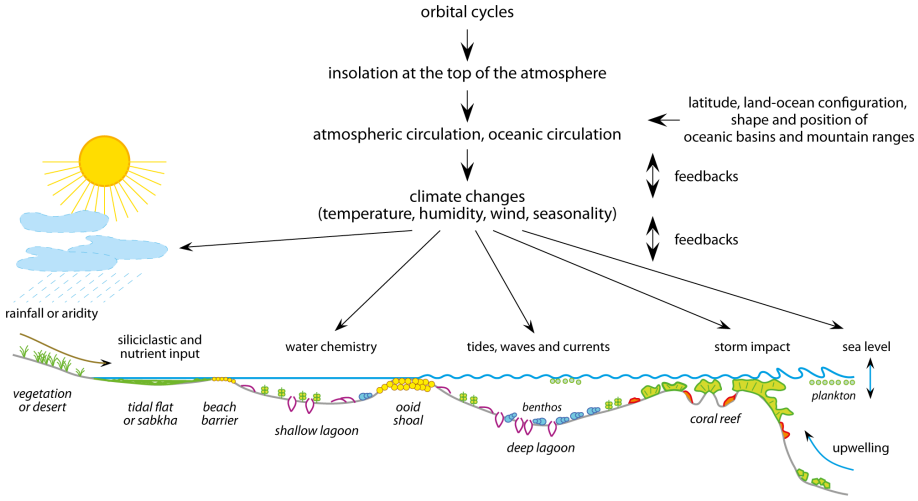

Figure 2. Chain of factors that influence a hypothetical, subtropical, shallow marine carbonate platform, including feedback processes. Amplitudes and frequencies of these factors may vary through time. The idealized cross section includes typical carbonate-producing environments (modified from Strasser, 2018).

Neth, 1997; Church and Clark, 2013; Sames et al., 2016; Ray et al., 2019).

If it can be shown that the physical and ecological parameters reigning over a sedimentary system were controlled by climate, and assuming that climate was at least partly controlled by orbital cycles, then a time resolution of the order of the shortest such cycles, which is the precession cycle of about 20 kyr, becomes possible. This is still far from the day-to-day monitoring of Anthropocene climate changes or of the yearly to centennial time resolution obtained for the Holocene, but it is better than the million-year scales that are proposed in many Mesozoic palaeoclimate models (e.g. Sellwood et al., 2000). In the following, the potential of shallow marine carbonates as recorders of orbitally controlled climate changes will be illustrated with an example from the Oxfordian of the Swiss Jura Mountains.

2 Oxfordian case study

2.1 Stratigraphy and palaeogeography

The Oxfordian sedimentary rocks in the Swiss Jura Mountains have been well studied by Gygi (1995, 2000). He established a lithostratigraphic scheme and dated it biostratigraphically by numerous ammonites (Fig. 3). In addition, Gygi et al. (1998) defined sequence boundaries that are correlated with the boundaries found in the chart of Hardenbol et al. (1998) that summarizes the sequence stratigraphy of

European basins. In the present study, the focus is on the interval between sequence boundaries Ox 6 and Ox 8 (Fig. 3).

The numerical ages of sequences and ammonite zones used in the chart of Hardenbol et al. (1998) are taken from the work of Berggren et al. (1995). The base of the Oxfordian there is dated at 159.4 ± 3.6 Ma and its top at 154.1 ± 3.2 Ma, implying a duration of about 5.3 Myr, albeit with wide error margins (Fig. 4). The ages of ammonite zones and sequence boundaries are interpolations between these values. Strasser et al. (2000) and Strasser (2007) performed a cyclostratigraphic analysis of Oxfordian platform sections and noticed that the sequences identified by Hardenbol et al. (1998) in many European basins actually correspond to sequences that formed in tune with the 405 kyr long eccentricity cycle or multiples thereof (Fig. 4). In the Geologic Time Scale (GTS) of 2012, Ogg et al. (2012) revised the duration of the Oxfordian, making it last 6.2 Myr. In the GTS of 2020, Hesselbo et al. (2020) attributed a still longer time interval of 6.75 Myr to the Oxfordian. Based on the analysis of several deep-water sections and aligned with the biostratigraphy and chronostratigraphy of Ogg et al. (2016), Huang (2018) counted three 405 kyr cycles in the interval between sequence boundaries (SB) Ox 6 and Ox 8. The discrepancies in radiometric dating are quite large and preclude a precise attribution of ages to the interval studied here. Furthermore, in the GTS 2020 the sequences boundaries are not dated, and there are differences in the position of sequence boundaries with respect to ammonite zones between the charts of Hardenbol et al. (1998) and Ogg et al. (2012). Also, the upper boundary of the Oxfordian has been shifted from the top of the Planula zone (Hardenbol et al., 1998) to the middle of the Bimammatum zone (Ogg et al., 2012) and finally to the base of the Bimammatum zone (Hesselbo et al., 2020; Fig. 4). Because the biostratigraphy and lithostratigraphy of Gygi (1995, 2000) agree with the biostratigraphy of Hardenbol et al. (1998), their scheme is adopted here. According to Ogg et al. (2012), sequence boundary Ox 7 sits in the middle between Ox 6 and Ox 8, but Strasser (2007) proposed a control by the long eccentricity cycle with a duration of 800 kyr between SB Ox 6 and Ox 7 and 400 kyr between SB Ox 7 and Ox 8 (Fig. 4). For the purpose of the present study it is important that the duration of the interval between SB Ox 6 and Ox 8 appears to be relatively stable: Hardenbol et al. (1998) attributed 155.81 Ma to SB Ox 6 and 154.63 to SB Ox 8, implying a duration of 1.18 Myr. Basically, the same value (1.2 Myr) was found by Strasser (2007) and Huang (2018). Ogg et al. (2012) dated SB Ox 6 at 159.4 Ma and SB Ox 8 at 158.2 Ma, also making the interval 1.2 Myr long. Consequently, this duration will be applied in the present study.

In the Oxfordian, the Jura platform was part of the wide passive margin to the north of the Tethys ocean. This margin was a complex array of shallow and deeper marine areas, with several emergent Hercynian massifs that were surrounded by siliciclastic aprons (Carpentier et al., 2006; Fig. 5). The platform was structured by synsedimentary faults (Allenbach, 2001; Strasser et al., 2015). Its palaeolatitude was 26 to 27° N (Dercourt et al., 1993), corresponding to the subtropical climate belt.

The average global climate during Oxfordian times was that of a greenhouse world; i.e. large polar ice caps were absent. Consequently, orbitally induced sea level changes were of low amplitude (see Sect. 1). Late Jurassic climate models have been proposed by e.g. Weissert and Mohr (1996), Rais et al. (2007), and Louis-Schmid et al. (2007), and a general circulation model has been developed by Sellwood and Valdes (2008). These models, however, only indicate million-year trends and do not consider high-frequency climate fluctuations in a restricted palaeogeographic area.

2.2 Definition and correlation of depositional sequences

Depositional sequences are defined here in terms of sequence stratigraphy (e.g. Catuneanu et al., 2009). Their formation is controlled by sea level changes. Sequence boundaries (SBs) form when sea level drops rapidly, which, on a shallow platform, may lead to subaerial exposure. Lowstand deposits are commonly very thin or absent on the platform because there is no room to accommodate the sediment. A transgressive surface (TS) forms when sea level rise leads to flooding of the platform, and the sediments above this surface then display a deepening-up trend (transgressive deposits). The fastest rise of sea level is indicated by the relatively deepest-water fauna and/or condensed deposits if sediment accumulation cannot keep up with sea level rise (MF: maximum flooding interval). Also, clays may accumulate below the wave base that has risen following the sea level rise. If a hardground develops or a rapid facies change occurs, a maximum flooding surface (MFS) can be defined. Slowing sea level rise then allows the sediment to fill the space created during maximum flooding, and a shallowing-up facies evolution is recorded (highstand deposits). A new sea level drop then terminates the sequence. These definitions are independent of the size of the sequences and the time involved in their formation (Mitchum and Van Wagoner, 1991; Strasser et al., 1999). Sea level changes may be local or regional (caused by tectonic uplift or subsidence) or global. The latter eustatic sea level fluctuations may be long-term (million-year scale caused by volume changes in ocean basins as a result of plate tectonics and basalt injections) or short-term (caused by orbital cycles; see Sect. 1).

The detailed analysis of facies evolution in the Oxfordian sections studied in the Swiss Jura Mountains allows defining depositional sequences of three different orders, which can be correlated between the sections. An exhaustive sequence stratigraphic and cyclostratigraphic analysis based on 19 sections covering the middle Oxfordian to late Kimmeridgian interval was carried out by Strasser (2007), but no palaeoclimatic interpretation was offered. For the purpose of the present study, only five sections covering the middle to late Oxfordian interval are presented (Figs. 6, 7). The Pertuis section is found where the road from Dombresson to

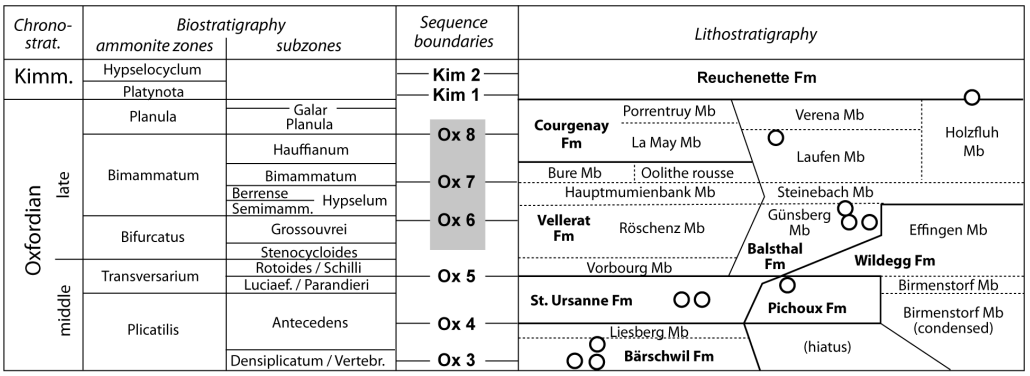

Figure 3. Stratigraphic scheme of the middle to late Oxfordian. Lithostratigraphy and biostratigraphy (white circles marking biostratigraphically significant ammonites) according to Gygi (1995, 2000). Sequence boundaries according to Hardenbol et al. (1998) and Gygi et al. (1998). Fm: formation; Mb: member; Kimm: Kimmeridgian. The focus of this study is indicated in grey.

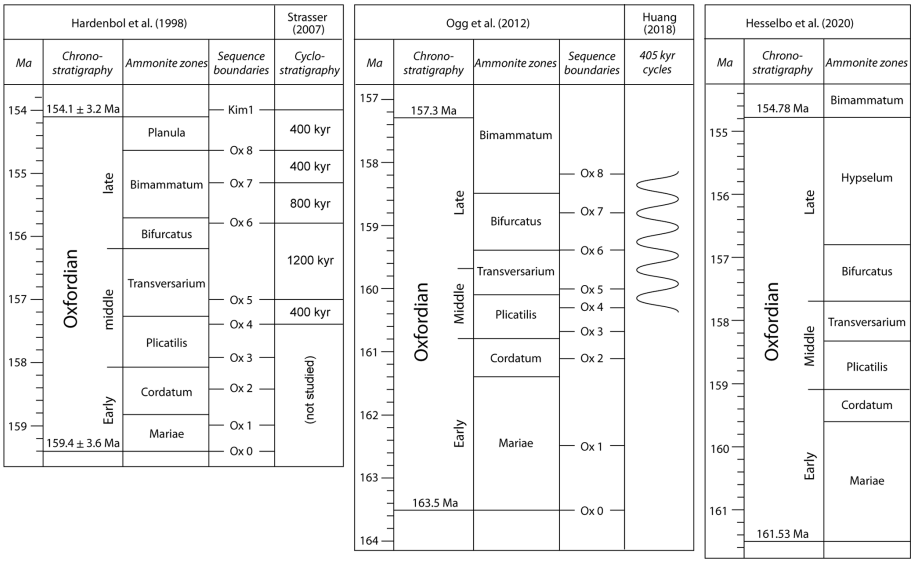

Figure 4. Comparison of three different timescales for the Oxfordian and cyclostratigraphic interpretations of Strasser (2007) and Huang (2018). Note that Strasser (2007) simplified the duration of the long eccentricity cycle to 400 kyr, while Huang (2018) used 405 kyr. For an explanation refer to the text.

St. Imier cuts through the Pertuis anticline (Pittet, 1996; Védrine, 2007). The La Chamalle section was studied by Jordan (1999) along a forest road towards La Chamalle farm to the northeast of the village of Péry-Reuchenette. The Péry-Reuchenette section was logged by Pittet (1996) and Hug (2003) in a quarry south of the village of Péry-Reuchenette at the exit of the canyon cutting through the first Jura anticline north of the city of Biel. The Gorges de Court section, studied by Hug (2003) and Védrine (2007), follows a footpath along the Birs River north of the Village of Court. The Hautes-Roches section was analysed by Dupraz (1999), Védrine (2007), and Stienne (2010). It runs along a forest trail southwest of the village of Hautes-Roches, north of Moutier.

The correlation lines of the depositional sequences in Fig. 7 are based on the interpretation of facies and sedimentary structures as explained above. The biostratigraphy established by Gygi (1995, 2000; see Fig. 3) allows correlating three of the five prominent sequence boundaries shown in Fig. 7 with the boundaries defined in European basins by Hardenbol et al. (1998), i.e. Ox 6, Ox 7, and Ox 8. The prominent transgressive surface at the base of the Hauptmumienbank and Steinebach beds is situated in the Semimammatum subzone (lowermost Bimammatum zone; Fig. 3) and formed shortly after the beginning of a major million-year-scale transgressive trend identified by Hardenbol et al. (1998) at the limit between the Bifurcatus and Bimammatum ammonite zones. Assuming that the time interval between Ox 6 and Ox 8 represents about 1.2 Myr (Fig. 4), it is suggested that each of the four prominent sequences shown in Fig. 7 represents 400 kyr (termed medium-scale sequences;

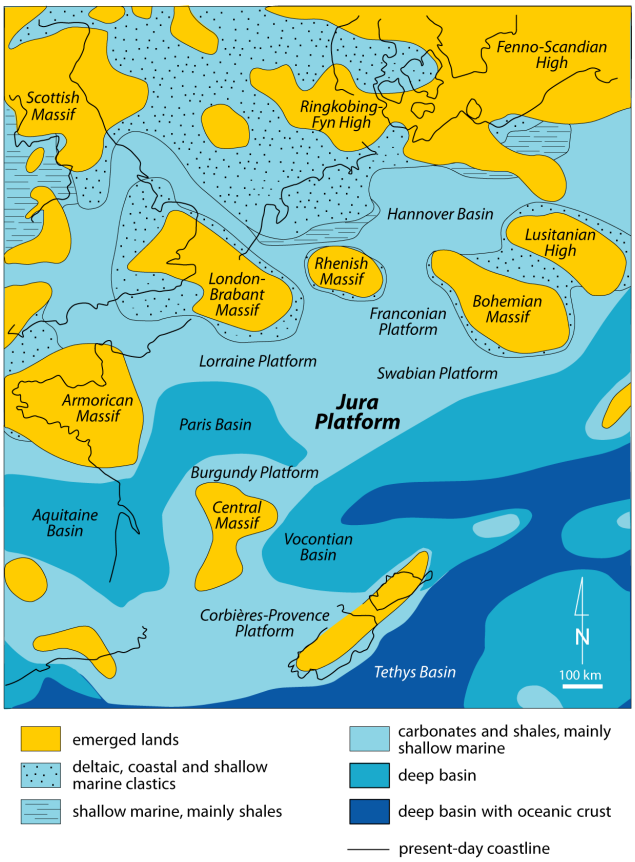

Figure 5. Palaeogeographic setting of the Jura platform during the Oxfordian. Modified from Carpentier et al. (2006).

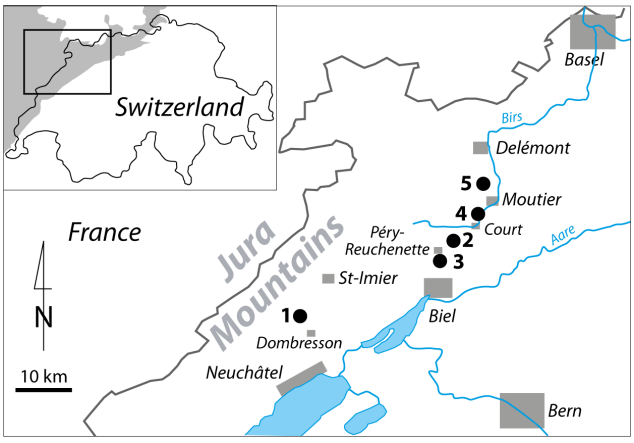

Figure 6. Locations of the sections presented in Fig. 7. 1: Pertuis; 2: La Chamalle; 3: Péry-Reuchenette; 4: Gorges de Court; 5: Hautes-Roches. Grey shade in the inset: Jura Mountains in France and Switzerland.

Strasser, 2007). Each 400 kyr sequence is composed of four small-scale sequences, implying that these lasted 100 kyr. Considering the hierarchical stacking pattern of these sequences and the timing, it is proposed that they formed in tune with orbital cycles: 405 kyr for the long eccentricity cycle and 100 kyr for the short one (note that, for simplification, the value of 400 kyr is used for the medium-scale sequences, although they formed in tune with the 405 kyr long eccentricity cycle). These long eccentricity cycles have also been found to be dominant in the early to middle Oxfordian Terres Noires Formation in southeastern France (Boulila et al., 2010). The medium- and small-scale sequences correlate well across the entire Jura platform (Strasser et al., 2015), implying that the sea level changes at the 405 and 100 kyr scales affected the entire carbonate platform, despite the facies mosaics and the morphological irregularities (Fig. 2).

The small-scale sequences are composed of individual beds, the number of which varies between 2 and 20 per small-scale sequence (Figs. 7, 8). These individual beds are more difficult to attribute to an orbital frequency (obliquity or precession) because, on the shallow platform, local processes such as lateral migration of sediment bodies could also have produced beds, independent of orbitally controlled sea level changes (e.g. Pratt and James, 1986; Strasser, 1991). Also, hiatuses were frequent, hampering a straightforward interpretation of such high-frequency cyclicity (e.g. Sadler, 1994; Strasser, 2015). However, many individual beds show a deepening–shallowing facies evolution that can be interpreted as resulting from a sea level cycle (e.g. Strasser et al., 1999). Many bed limits are underlined by thin marly layers, which reflect a more humid climate and/or a sea level drop that washed clays into the sedimentary system. If, in addition, a small-scale sequence is composed of five such well-defined beds, these can be attributed to the 20 kyr precession cycle and are called elementary sequences. Sub-Milankovitch cycles, i.e. cycles with frequencies shorter than those of the precession cycle, have been described and interpreted for shallow and deep marine successions (e.g. Zühlke, 2004; de Winter et al., 2014), but there is no evidence for such cycles in the studied Oxfordian sections.

Figure 8 shows an example of correlation of elementary sequences between the sections of Fig. 7. The prominent transgressive surface at the base of the Hauptmumienbank and Steinebach members is found all over the Swiss Jura (Gygi, 1995; Védrine and Strasser, 2009). It overlies marly sediments that locally contain fully marine fauna (echinoderms, brachiopods) mixed with freshwater algae (charophytes), suggesting that the sediment deposited during the sea level lowstand terminating the previous sequence was reworked in the early phases of the transgression (Védrine, 2007). The rapid shift to carbonates then implies that the whole platform was flooded and siliciclastic input was stopped. Elementary sequences are defined by prominent bedding surfaces and/or by rapid shifts in facies. The sequence boundary of the small-scale sequence (also shown in Fig. 7) in Gorges de Court is furthermore marked by birdseyes that formed on a tidal flat and by siliciclastics in Pertuis and Hautes-Roches. The abrupt termination of carbon-

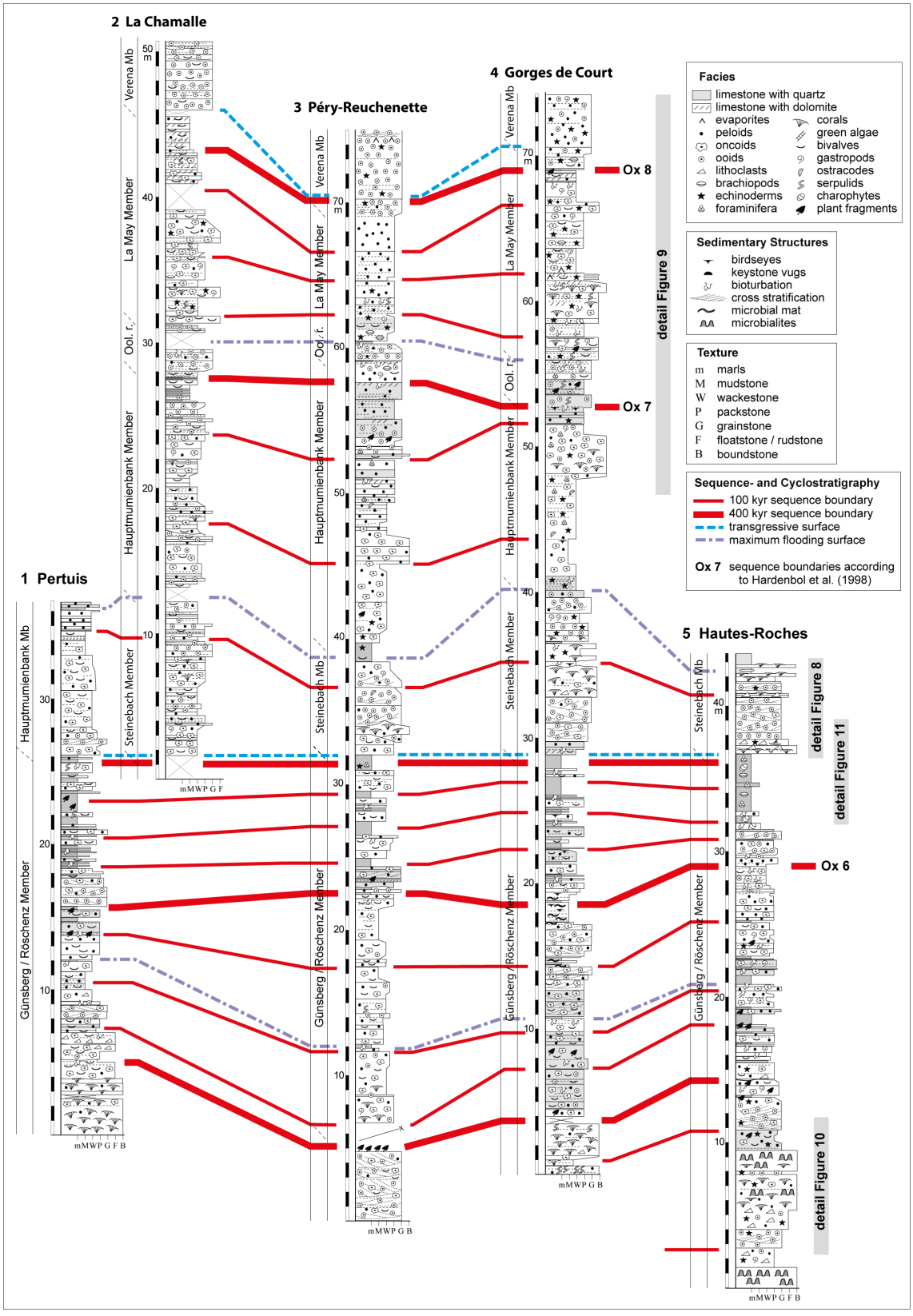

Figure 7. Facies evolution and correlation of five sections logged in the Swiss Jura Mountains (based on Strasser, 2007). Texture terminology according to Dunham (1962) and Embry and Klovan (1971). For explanations refer to the text.

ate sedimentation and the input of clays are interpreted as representing a maximum flooding surface, which is that of the medium-scale, 400 kyr sequence leading up to sequence boundary Ox 7 (Fig. 7). Between the prominent transgressive surface and the small-scale sequence boundary, five elementary sequences are counted in four of the sections. Péry-Reuchenette is dominated by oolites, which formed on constantly shifting shoals and where the formation of clear sequence boundaries was precluded. The sections of Pertuis and La Chamalle are dominated by oncoids that formed in lagoons, while the other three sections display oolites and coral reefs. The reefs did not develop at the same time in these sections, which is explained by the facies mosaics and the shifting depositional environments as illustrated in Fig. 2. One elementary sequence may correspond to several beds visible in the outcrop. This is due to reactivation surfaces in high-energy shoals and to localized shifting of sediment bodies by currents and waves in low-energy lagoons. The differences in thickness of the small-scale sequence are related to the faulted structure of the platform (Strasser et al., 2015): quiet-water lagoons formed behind high-energy ridges where reefs built up and ooid shoals developed, as well as where the preservation potential was less (Fig. 2).

In the following, three examples chosen from the sections in Fig. 7 will be discussed in detail.

2.3 Description and interpretation of characteristic sections

2.3.1 Gorges de Court

This detailed section (Fig. 9) has been chosen because it represents a well-developed stacking pattern reflecting the orbital cycles. It starts with wackestones of a low-energy, protected lagoon, followed by a boundstone composed of corals and oncoids in the Hauptmumienbank (meaning "main mummy bed", referring to the oncoids). Corals indicate warm, oligotrophic conditions, and both corals and echinoderms point to normal marine salinity. Oncoids form in lagoons with high microbial activity. The top of this bed is slightly dolomitized, suggesting shallow water and semiarid conditions. This is where a first sequence boundary can be placed.

The following part of the section is characterized by terrigenous components (up to 5 % quartz, feldspar, and terrestrial organic matter). At the top of the fourth thin bed, birdseyes point to a tidal flat, and a second SB can be placed there. The facies is reddish, and the ooids explain the name of Oolithe rousse Member. This whole interval points to generally low sea level, albeit with high-frequency fluctuations in water depth to explain the passage from tidal flat to ooid bar. The siliciclastics originated from erosion in the hinterland under a humid climate, and low sea level favoured their progradation into the lagoon. The terrigenous organic matter equally suggests a humid climate, allowing for growth of vegetation, in contrast to the dolomite just below.

Above follow facies varying between bioturbated packstones (low water energy) and grainstones (high energy). The main components, ooids, oncoids, bivalves, and serpulids, all imply lagoonal conditions. Corals, commonly encrusted by microbialites, become dominant in the middle part of the section, where the individual beds are also thickest (up to 1.8 m). Nevertheless, several bed tops in this interval show dolomitization, suggesting rapid changes between sea level rise to accommodate the coral patch reefs under fully marine conditions and by sea level drops to allow for penecontemporaneous dolomitization on tidal flats. Between metres 15 and 16, even some pseudomorphs after anhydrite are found, pointing to an arid climate.

The facies above the coral-rich interval are dominated by oncoids, which formed in protected, low-energy lagoons (wackestones, packstones, and floatstones). Tidal flats still occur in the lower part of this interval. Echinoderms and brachiopods point to normal marine salinity. The strongly bioturbated surface at metre 20.6 is interpreted as a maximum flooding surface: no sedimentation for a certain time and several generations of organisms that burrowed through the seafloor. An important change occurs at metre 21.3 of this section: after an intensely dolomitized tidal flat, two 2 to 3 cm thick layers rich in terrigenous organic matter imply the formation of marshes and ponds, in which marginal marine vegetation could grow. The climate must have changed rapidly from arid or semiarid to humid. Sea level was low and allowed the formation of a major sequence boundary. After this important sequence boundary, sea level rose to accommodate a fully marine lagoon with brachiopods and echinoderms and then thick-bedded, high-energy ooid and peloid bars.

According to Gygi (1995), the Oolithe rousse Member belongs to the Bimammatum subzone (Fig. 3) and thus also contains SB Ox 7 of Hardenbol et al. (1998). The organic-rich layers at metre 21.3 occur in the upper part of the La May Member, which corresponds to the limit between the Bimammatum and Planula zones and thus to SB Ox 8 (Fig. 3). According to the sequence- and cyclostratigraphic interpretation of the Jura platform by Strasser (2007), the interval between SB Ox 7 and Ox 8 corresponds to about 400 kyr (Fig. 4). This is close to the value of the long eccentricity cycle (405 kyr), and it can thus be postulated that this major sequence observed at Gorges de Court formed in tune with this orbital cycle.

While SB Ox 8 is represented by two thin layers rich in terrestrial organic material testifying to a sea level drop, SB Ox 7 is less well defined. It has been interpreted at the top of the bed with birdseyes (indicating a tidal flat) at metre 6.2, but the entire siliciclastic-rich interval implies low sea level. This is why a sequence boundary zone is indicated in Fig. 9, corresponding to a time interval that favoured the formation of surfaces that qualify as sequence boundaries (Montañez

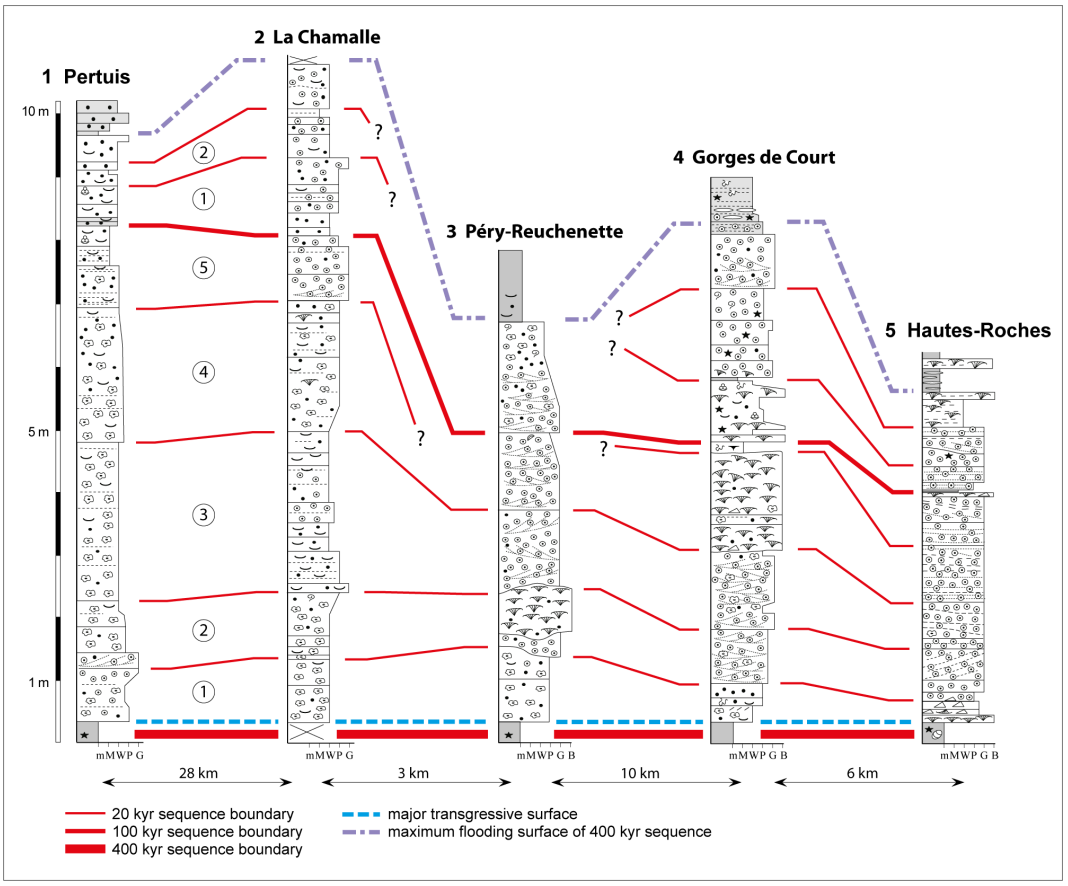

Figure 8. Correlation of elementary sequences between the prominent transgressive surface forming the base of the Hauptmumienbank and Steinbach members as well as the maximum flooding surface of the corresponding medium-scale sequence (based on Védrine, 2007). For discussion refer to the text.

and Osleger, 1993; Strasser et al., 1999). The same holds for the maximum flooding zone in Fig. 9: the thickest beds and most open marine facies define an interval where sea level rose rapidly to create accommodation and fully marine conditions. SB Ox 7 and Ox 8 as well as the maximum flooding zone correlate well with other sections on the Swiss Jura platform (Strasser, 2007; Fig. 7).

Between SB Ox 7 and Ox 8, 22 beds are counted (Fig. 9). These beds are separated by thin layers of marls, the clays having been washed into the system during high-frequency sea level drops and/or during phases of more rainfall in the hinterland. Thus, they qualify as elementary sequences, even if their facies do not always display deepening then shallowing-up trends (Strasser et al., 1999). 405 kyr divided by 22 results in 18.4 kyr, which is close to the 20 kyr duration of the orbital precession cycle in the Oxfordian (Berger et al., 1992). Considering the complexity of the translation of orbitally induced insolation cycles into the sedimentary system (Fig. 2) and considering the possibility of local processes potentially creating beds, it is not astonishing that the fit is not perfect.

The identification of the small-scale sequences reflecting the short eccentricity cycle of 100 kyr in this outcrop is not easy. Their boundaries are not well developed and are mainly inferred from correlation with other sections (Fig. 7; Strasser, 2007). In Fig. 9, they correspond to rapid changes from high-energy grainstone or floatstone facies (implying shallower water with waves and currents) to low-energy wackestone or packstone facies formed below wave base (thus implying an increase in water depth). Following these criteria, four such sequences are counted within the 400 kyr sequence. The small-scale sequences are composed of four to six individual beds. Again, the perfect fit would have been five beds per sequence, but the sedimentary system was complex and did not always translate the orbital cyclicity one-to-one.

2.3.2 Hautes-Roches A

In the Hautes-Roches section, two coral-rich intervals are encountered (Fig. 7; Dupraz, 1999). The lower one (Fig. 10) corresponds to a small-scale sequence that formed in tune with the 100 kyr eccentricity cycle. In this outcrop, the boundaries of the sequence are defined by sharp transgressive

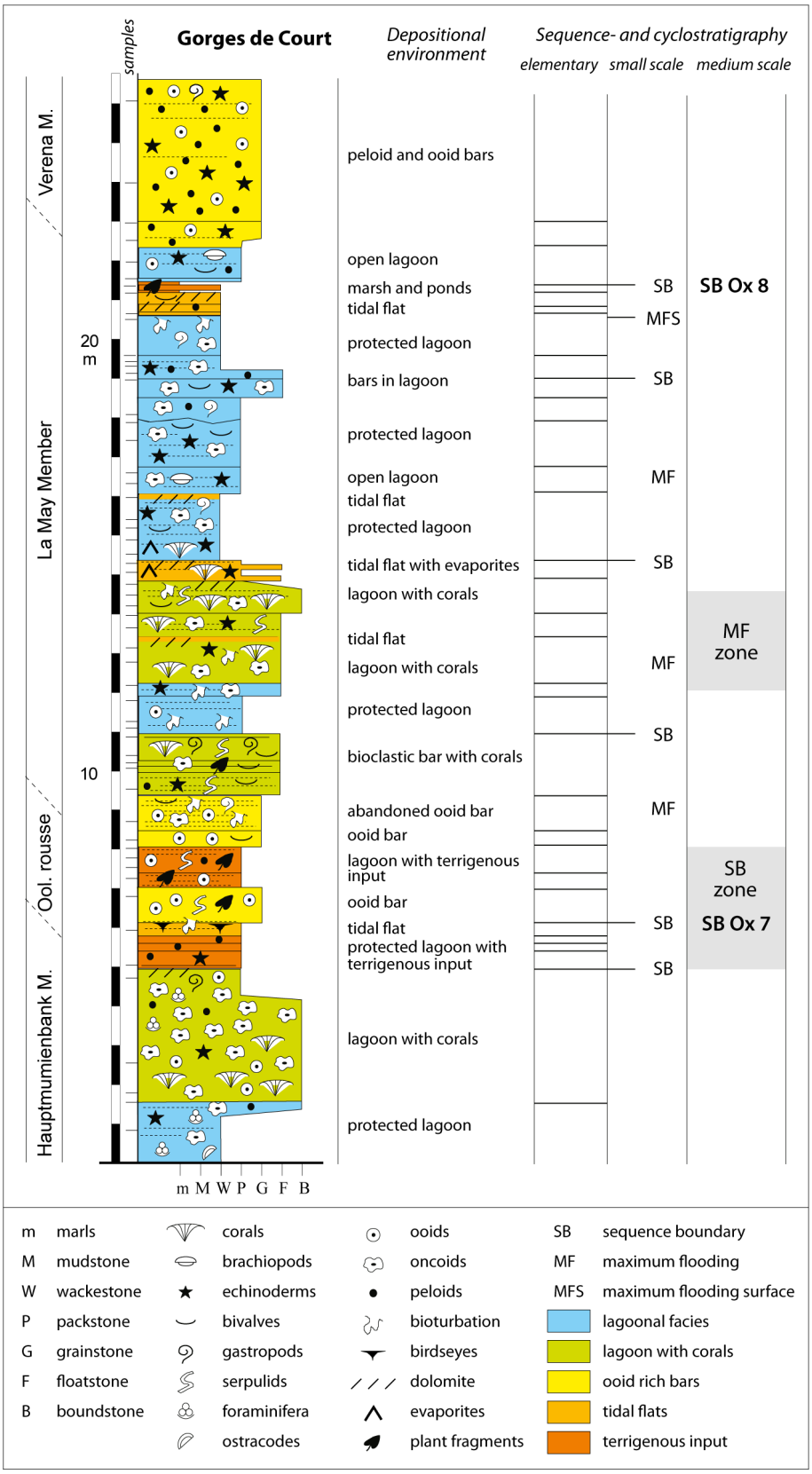

Figure 9. Detail of the Gorges de Court section. Log and facies are according to Hug (2003), and the sequence stratigraphic and cyclostratigraphic interpretation is based on Strasser et al. (2000). Ool. rousse: Oolithe rousse Member. For discussion refer to the text.

surfaces (TSs), which superpose cross-stratified ooid grainstones over lagoonal sediments (the sequence boundaries are hidden in the sediments just below the TSs or amalgamated to them; Strasser et al., 1999). This suggests that, at the beginning of a sea level rise, ooid shoals migrated over lagoons. The bed above the first ooid shoal still contains ooids but also coral debris, suggesting that a nearby coral reef was being dismantled by storms. Healthy corals then grew on top of the rubble, implying increasing water depth. Later, the corals adopted a flat shape, possibly because they had to increase their surface to catch enough light for the photosynthetic zooxanthellae, which again points to increasing water depth. Coral diversity was high (mainly *Microsolena, Heliocoenia, Stylina, Isastraea*, and *Calamophylliopsis*; Dupraz, 1999). The corals gradually became covered by microbialites, which implies increased nutrient input and eutrophication of the system (Hallock and Schlager, 1986; Dupraz and Strasser, 2002). A sharp surface terminates this bed. Above, coral growth sets in again, but the corals are covered by microbialites, and oncoids are present. The Microsolenids in particular are associated with microbialites, suggesting that this family supported some degree of eutrophication. A washover deposit rich in echinoderms interrupted the growth of this reef, implying that a major storm passed over it. Above a last large coral head (probably not in situ but toppled) and flat corals, only microbialites are present; they have a thrombolite texture and include some sponges. This sequence, from ooid shoal through coral reef to thrombolite, suggests that water energy decreased through time, that the water became deeper and more turbid to hamper the photosynthesis of the coral symbionts, and that nutrient excess favoured microbial growth that eventually suffocated the corals.

This evolution ends with a bioturbated, nodular layer capped by a bored hardground, indicating that the seafloor was exposed over some time to become cemented and perforated by lithophaga bivalves. The hardground also marks the end of a deepening-up trend and is thus considered a maximum flooding surface (MFS). Above the hardground, brachiopods indicate normal marine salinity. Quartz sand and (in the upper part of the bed) plant debris testify to terrigenous input and progradation of lagoonal sediments. These is interpreted as shallowing-up highstand deposits. A thin bed with echinoderms (possibly a tempestite) and a new ooid shoal then represent the beginning of a new sequence.

The sequence is composed of seven beds. One, however, is an event deposit (the washover), and one belongs to the composite hardground covering the thrombolite. Considering the architecture of depositional sequences observed on the Jura platform where the transgressive parts of small-scale sequences are commonly composed of limestones while the regressive highstand parts are in many cases marly (Strasser et al., 2015), it is suggested that the sequence shown here corresponds to the 100 kyr short eccentricity cycle and that the formation of each bed was controlled by the orbital precession cycle of 20 kyr. The bed limits are transgressive surfaces or maximum flooding surfaces; the sequence boundaries are not developed (Strasser et al., 1999). The washover deposit that served as a substratum for renewed coral growth is attributed to elementary sequence 4, but the storm event may also have occurred at the end of sequence 3. During the first four precession cycles, conditions were those of a gradual transgression, which ended in the hardground. The highstand deposits took only 20 kyr to form, making the record of this 100 kyr cycle highly asymmetrical.

2.3.3 Hautes-Roches B

The second interval at Hautes-Roches shown here is dominated by lagoonal marls. The section illustrated in Fig. 11 starts with a firmground that covers lacustrine mudstones to wackestones with charophytes. Above, a first thin bed still has lacustrine facies. The following thin bed contains charophytes as well as marine fossils, implying a marine, transgressive pulse that reworked lacustrine elements. A second transgressive surface then leads to a strongly bioturbated lagoon. The next 2 m contain echinoderms and brachiopods, implying normal marine salinity. Three nodular beds are found in this interval. They are thickening up, and quartz content increases upwards to up to 20 % (Stienne, 2010). This evolution is typical of a shallowing-upwards highstand deposit. In this case, the maximum flooding interval can be placed at the strongly bioturbated bed, while a sequence boundary is identified at the base of the third nodular bed (Fig. 11). Five elementary sequences are identified, leading to the hypothesis that they correspond to the 20 kyr precession cycle and the small-scale sequence they make up to the 100 kyr short eccentricity cycle. This small-scale sequence is also found in the other sections shown in Fig. 7. Each of the elementary sequences has a lower carbonate-rich part interpreted as transgressive deposits and a siliciclastic-rich upper part that represents the highstand deposits.

The following 1.2 m are composed of lagoonal marls with a fully marine fauna. They are covered by a sharp transgressive surface, above which grew a reef composed of small corals. This same transgressive surface is illustrated in Fig. 8. It marks the base of the coral- and ooid-rich Steinebach Member and of the oncoid-bearing Hauptmumienbank Member, respectively (Fig. 3). The corresponding sequence boundary is hidden in the marls below the TS, as suggested by the presence of freshwater charophytes mixed with marine fauna (Védrine, 2007). Elementary sequences cannot be recognized.

Reef development in this section was short-lived. Above the thin reefal boundstone with low coral diversity (mainly *Isastraea* and *Microsolena*; Dupraz, 1999), only reworked coral clasts appear that, however, suggest that reef growth continued in the neighbourhood. The phase of reef development was then interrupted by ooid shoals, one of which displays sigmoidal cross-beds formed by tidal currents.

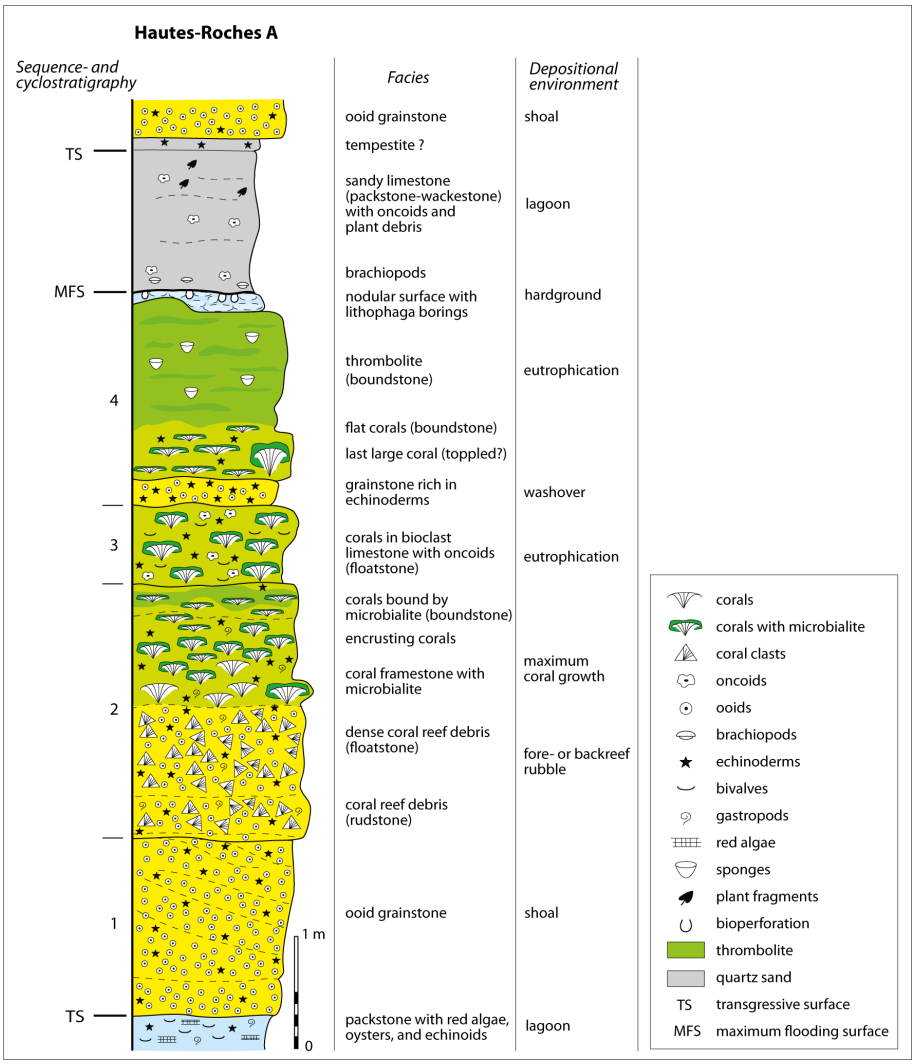

Figure 10. Detail of the Hautes-Roches section A. Log and facies based on Dupraz (1999). For discussion refer to the text.

3 Discussion

Although the climate factors influencing a shallow marine carbonate platform are intimately linked (Fig. 2), they will be discussed here separately.

3.1 Water temperature

In ancient carbonates, oxygen isotope ratios are often used as a proxy for the temperature of the water in which they formed. This, however, requires that the original mineralogy be preserved in the fossil record. In shallow marine carbonates, this is rarely the case: early freshwater diagenesis dissolves the aragonite of corals, gastropods, and green algae, and the high-Mg calcite of echinoderms is transformed into low-Mg calcite. An exception are brachiopod shells, which have a relatively stable low-Mg calcite composition and are found in the studied sections. However, the $\delta^{18}O$ values that are recorded also depend on the geochemistry of the platform waters, which may vary considerably across a complexly structured platform such as the one in the Jura Mountains (e.g. Immenhauser et al., 2003; Colombié et al., 2011).

Among the tropical and subtropical carbonate-producing organisms, corals are the most sensitive to temperature changes. Today, reef-building zooxanthellate corals do not support water temperatures below 18 °C and above 34 °C (Wood, 1999). For short periods, however, they tolerate fluctuating and even higher temperatures (e.g. Schoepf et al., 2015). Aragonite saturation in seawater, which is important for efficient coral skeleton formation, closely follows water temperature (Wood, 1999). If it is assumed that Oxfordian corals had the same requirements regarding temperature as the recent ones, a high-diversity reef would be a proxy for water temperatures ranging from about 23 to 29 °C. In the middle and late Oxfordian, coral reefs were widely distributed between the palaeolatitudes of 40° N in Japan to

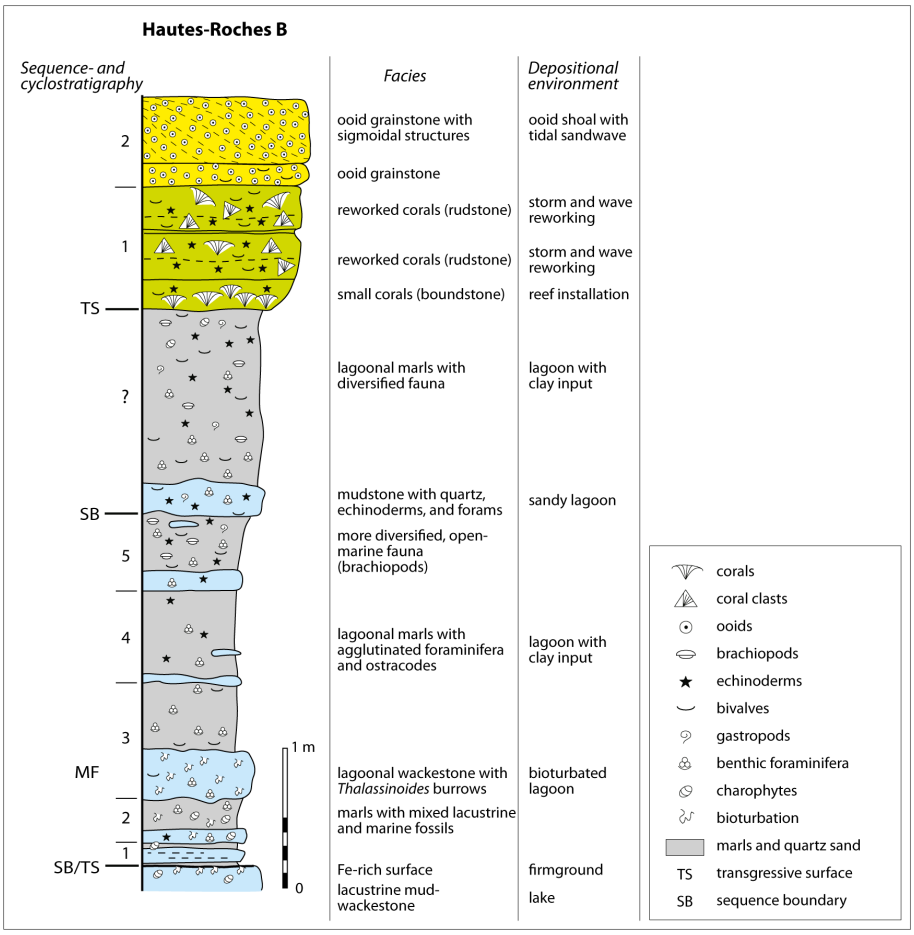

Figure 11. Detail of the Hautes-Roches section B. Log and facies based on Dupraz (1999) and Stienne (2010). For discussion refer to the text.

45° S in the Neuquén Basin (Leinfelder et al., 2002) where these water temperatures were common. The reef in the Hautes-Roches section (Fig. 10) with a relatively high coral diversity may thus indicate water temperatures between 23 and 29 °C. Low diversity, however, may not only be an effect of temperature but also of other unfavourable conditions such as water that is too shallow or too deep, high sediment input that makes the water turbid and thus hinders photosynthesis of the symbionts, nutrient excess that favours microbialites and fleshy algae that compete with the corals, or water acidification that impacts skeletal growth.

Based on a mean value of $-3.50\,‰\,\delta^{18}O$ in micritic whole rock (which averages the isotopic signal of the different components) from middle Oxfordian sections in the Swiss Jura, Plunkett (1997) calculated ambient water temperatures of 26 to 27 °C (following Anderson and Arthur, 1983). This compares well with Frakes et al. (1992), who indicate up to 27 °C for late Oxfordian ocean surface temperatures according to oxygen isotope ratios measured on planktonic foraminifera and belemnites. Martin-Garin et al. (2010) measured oxygen isotope ratios on brachiopods and oysters from outcrops in the Swiss Jura. They calculated water temperatures of below 20 °C for the low-diversity coral reefs (15 genera) in the Liesberg Member (Fig. 3), about 25 °C for the high-diversity reefs (37 genera) in the St. Ursanne Formation, and about 20 °C in the Günsberg Member where coral diversity declined (13 genera). The reef complex shown in Fig. 10 is situated in this latter member.

For the carbonate platform in the French Jura, Olivier et al. (2015) interpreted a climate evolution going from warm and humid to warm and arid in the course of the Bimammatum zone. This corresponds to the time interval between sequence boundaries Ox 6 and Ox 8 discussed here (Fig. 3). In the Paris Basin, Brigaud et al. (2014) cite sea surface temperatures of 20 to 29 °C for the Late Jurassic, with an optimum during the middle Oxfordian. At the onset of the late Oxfordian, water temperatures dropped by 6 to 7 °C, and rainfall increased. Carpentier et al. (2010) state that, in the eastern Paris Basin, after a warm and arid interval favouring carbonate production in the Transversarium zone, the climate became cooler and more humid in the Rotoides and Stenocyloides subzones. In the southern North Sea, Abbink

et al. (2001) analysed sporomorphs as palaeoclimate proxies and showed that there was a temperature drop between the boreal Serratum and Regulare ammonite zones. This corresponds to the Semimammatum subzone in the Tethyan realm (Fig. 3), in which the major transgressive surface is situated and in which coral reefs began growing (Figs. 7, 8). It thus appears that, while the water temperature in the Tethys ocean increased, the North Sea was cool.

3.2 Sea level

Sea level changes in the Milankovitch frequency band are an important proxy as they reflect changes in global air and water temperature. During the Quaternary, glaciation cycles controlled by the 100 kyr short eccentricity cycle led to important asymmetrical sea level fluctuations due to slow buildup of ice caps followed by rapid melting (Shackleton, 1987; Fig. 13). In greenhouse worlds, i.e. when major ice caps were absent, the translation of orbitally controlled insolation changes into eustatic sea level changes was more direct. Thermal expansion and retraction of ocean surface water were important factors controlling sea level fluctuations, in tune with the eccentricity cycles of 100 and 405 kyr (Sames et al., 2016). Schulz and Schäfer-Neth (1997) proposed that thermally induced volume changes in deep-water circulation resulted in sea level changes. Water storage and release on the continents (aquifer eustasy; Jacobs and Sahagian, 1993; Sames et al., 2014; Wendler and Wendler, 2016) depend on the climate over the land areas: sea level rise is linked to a drier climate with less precipitation, when aquifers empty more rapidly than they fill up. Consequently, aquifer eustasy is dependent on the latitudes at which the land areas occur and on the atmospheric circulation cells; i.e. it is also controlled by the obliquity and precession cycles. Obliquity is dominant at high latitudes and cannot be identified in the studied sections. The 20 kyr precession cycles, on the other hand, are potentially recorded in the elementary sequences.

For Cretaceous high-frequency sea level cycles, Davies et al. (2020) proposed the combined effects of thermal expansion, glacioeustasy, and aquifer eustasy to produce the 65, 30, and 50 m amplitudes observed in the Valanginian, Turonian, and Maastrichtian, respectively. Aquifer eustasy taken alone would be responsible for amplitudes of less than 5 m, which is in the range of the reconstructed Oxfordian amplitudes (see below). Wendler et al. (2016) suggested that aquifer eustasy could drive sea level changes even of the order of 30 to 40 m at the frequency of the long eccentricity cycle that shifted the Hadley circulation and the width of the equatorial humid belt.

For the part of the Gorges de Court section shown in Fig. 9, Strasser (2018) reconstructed a sea level curve that explains the observed stacking pattern of beds. For this, the section was first decompacted according to facies (Goldhammer, 1997; Strasser and Samankassou, 2003). The following decompaction factors are applied: 1.2 for grainstones, 1.5 for packstones, 2 for wackestones, 2.5 for mudstones, and 3 for marls. Boundstones have resisted compaction, and a factor of 1.2 is used. Floatstones with their micritic matrix are treated like packstones. Estimation of water depth for the different facies of course is not easy: the facies depend not only on water depth but also on water energy, and the same facies may be present over a wide depth range. For this exercise, the following values have been assumed: tidal flats form within the tidal range and are set at 0 m. These are the tie points on the reconstructed curve (Fig. 12). Grainstones often result from winnowing by waves and currents, and a water depth of 1 m is attributed. Packstones and floatstones with abundant fauna are set at a minimum of 2 m. Coral patch reefs can potentially grow up to sea level but are assumed to have needed at least 2 m water depth to develop. When an open marine fauna (e.g. brachiopods) is present, a minimum water depth of 3 m is assumed. By this, only trends in the evolution of water depth are reconstructed, and no error bars are applied. To accumulate the sediment pile between Ox 7 and Ox 8 (15.3 m today, 26 m when decompacted; Strasser, 2018), a gain in accommodation of 26 m is needed (Fig. 12). This is created by subsidence and long-term sea level rise. This long-term trend can be subdivided into four portions according to the space needed to accumulate the individual small-scale, 100 kyr sequences. Deducing these trends from the reconstructed sea level curve, the deviation of sea level change from the average accommodation gain can be visualized for each 100 kyr sequence. It is interesting to note that, for the medium-scale sequence, two candidates for a maximum flooding zone can be proposed, both situated in the interval of high accommodation gain (Fig. 12). However, when comparing with other sections in the Swiss Jura, it is rather the lower one that is recognized all over the platform (Strasser, 2007; Fig. 7).

Small-scale sequences 3 and 4 are well defined, and each contains five elementary 20 kyr sequences. Sequence boundary Ox 7, which defines the limit between small-scale sequences 0 and 1, is placed at the tidal flat. This results in only four elementary sequences for small-scale sequence 0 and six for small-scale sequence 1 (Fig. 12). This misfit may be explained by a wrong definition of the elementary sequences or by factors other than sea level that created a topographic high to install the tidal flat (differential subsidence, lateral migration of sediment bodies). The top of the second small-scale sequence (elementary sequence 14 in Fig. 12) shows corals, microbialites, and lithophaga borings but also evaporites, pointing to rapid changes in water depth. It is possible that the fifth elementary sequence was not recorded due to lack of accommodation.

The next step is to reconstruct the amplitudes of the highest-frequency sea level fluctuations corresponding to the 20 kyr precession cycle by subtracting the 100 kyr trends (Fig. 13). When compared to the envelope curve based on the calculated insolation changes at the Equator and for the last 550 kyr, a partial correspondence becomes visible: stronger insolation due to the 100 and 405 kyr cyclicity generally

translates into higher sea level amplitudes for the 20 kyr cycles. Even considering the complex facies distribution on a shallow marine platform and accommodation changes due to differential subsidence, and even considering the uncertainties in estimating decompaction factors and water depth, it can be concluded that, in the Oxfordian case discussed here, orbitally controlled insolation changes translated into sea level changes. The similarity of the symmetrical changes in amplitude at the 100 and 405 kyr scales between the reconstructed sea level fluctuations and the calculated insolation changes (Fig. 13) suggests that the translation from insolation to sea level was mainly via thermal expansion and retraction of the ocean surface water, which is a process that depends on air temperature. Aquifer eustasy and low-amplitude glacioeustasy were certainly present but are difficult to quantify in the present study.

It has to be kept in mind that the precession cycle today has a 21 and 23 kyr periodicity, while in the Oxfordian the periodicity was at about 20 kyr (Berger et al., 1992; Hinnov, 2018). The number of high-frequency cycles in Fig. 13 is therefore not the same for the Quaternary and Gorges de Court. On the other hand, the 100 and 405 kyr cycles are stable through time and can be directly compared. A synthesis of 12 Oxfordian sections in the Swiss Jura showed that many small-scale sequences controlled by the 100 kyr short eccentricity cycle are composed of a lower transgressive part dominated by high-energy, carbonate-dominated facies (e.g. ooid or bioclastic shoals, coral reefs), while the upper regressive part displays low-energy carbonate facies (e.g. tidal flats) or marls (Strasser et al., 2015). The conclusion is that during a warming climate sea level rise pushed back the terrigenous delivery, and clear, oligotrophic, warm, and deepening waters allowed for carbonate production and accumulation. During a cooler climate, sea level dropped, siliciclastics prograded, water depth diminished, and carbonate production was reduced. A cooler climate coincided with more rainfall (see below), thus reinforcing erosion on the land areas.

Pittet and Gorin (1997) analysed the palynofacies in the Vellerat Formation (Fig. 3). They found that the ratio between land-derived particulate organic matter (plant debris, pollen and spores) and marine particles (phytoplankton, foraminifer linings) reflects proximal to distal trends, which depended on the land–ocean configuration but also on sea level changes. The analysis of associations of benthic foraminifera at the Oxfordian–Kimmeridgian boundary in the Paris Basin by Lefort et al. (2011) revealed a correlation with sea level changes: a highly diversified association composed of small agglutinated and calcitic forms characterizes high sea level stands, while an association richer in large agglutinated foraminifera is abundant when sea level was low. Unfortunately, there is no indication of the duration of the sea level cycles.

1 °C of global warming today leads to 20 to 60 cm of sea level rise through thermal expansion of the ocean water (Church and Clark, 2013). If the same values are assumed for Oxfordian times, and if thermal expansion is considered the main factor, a sea level rise of 2 m (Fig. 13) would suggest an atmospheric warming of 3 to 10 °C. Insolation by itself would not have allowed for this warming, but its input was enhanced by feedbacks due to greenhouse gases. For example, Ikeda et al. (2020) suggested that ca. 10 Myr orbital variations controlled summer monsoon dynamics, which changed terrestrial weatherability, affected atmospheric pCO_2, and eventually led to variations in sea surface temperatures of the order of 3 to 7 °C. At the scale of obliquity cycles, Laurin et al. (2015) explained the $\delta^{13}C_{carb}$ signature in the Late Cretaceous English Chalk by recycling of carbon through formation and decay of reservoirs of organic matter and/or methane on land, in lakes, and in euxinic marine settings.

It is interesting to compare rates of sea level rise between the Oxfordian and today. Taking two examples from Fig. 12, it can be estimated that, to accommodate elementary sequence 5, sea level must have risen by about 2 m within 10 000 years (half a precession cycle) and by about 3 m for elementary sequence 9. This amounts to values of 0.2 mm per year for the first case and 0.3 mm yr^{-1} for the second one (under the condition that sea level change was mainly controlled by thermal expansion of the ocean water and thus followed a symmetrical curve). Based on the detailed analysis of one elementary sequence in the Röschenz Member, Strasser et al. (2012) estimated a rise of 0.3 mm yr^{-1} during maximum flooding, i.e. during the fastest rise of the sea level cycle. Today, due to anthropogenically induced global warming, global mean sea level rose by 3.7 mm yr^{-1} between 2006 and 2018 (Masson-Delmotte et al., 2022), i.e. more than 10 times faster than in the Oxfordian.

3.3 Rainfall

Terrigenous material (clays, quartz, feldspar, terrestrial organic matter) appears at regular intervals in the studied sections. Thin, only millimetre- or centimetre-thick marl layers commonly from the limits between individual beds, and several metre-thick intervals around sequence boundaries Ox 6 and Ox 7 are dominated by siliciclastics and contain plant fragments. The maximum flooding zone at metre 40 in the Péry-Reuchenette and Gorges de Court sections also contains clays and 1 % quartz (Fig. 7; Hug, 2003). According to the sequence stratigraphic interpretation, these intervals commonly correspond to low sea level stands, with the exception of the maximum flooding at metre 40. Falling sea level increases erosion of the hinterland, i.e. of the Hercynian massifs (Fig. 5). Deltas prograde, and terrigenous material is delivered into the lagoons. A second factor of course is rainfall in the hinterland, which activates the rivers that transport the siliciclastics and plant fragments towards the ocean. Input of aeolian quartz under an arid climate cannot be excluded, but transport by rivers is considered to have been the main

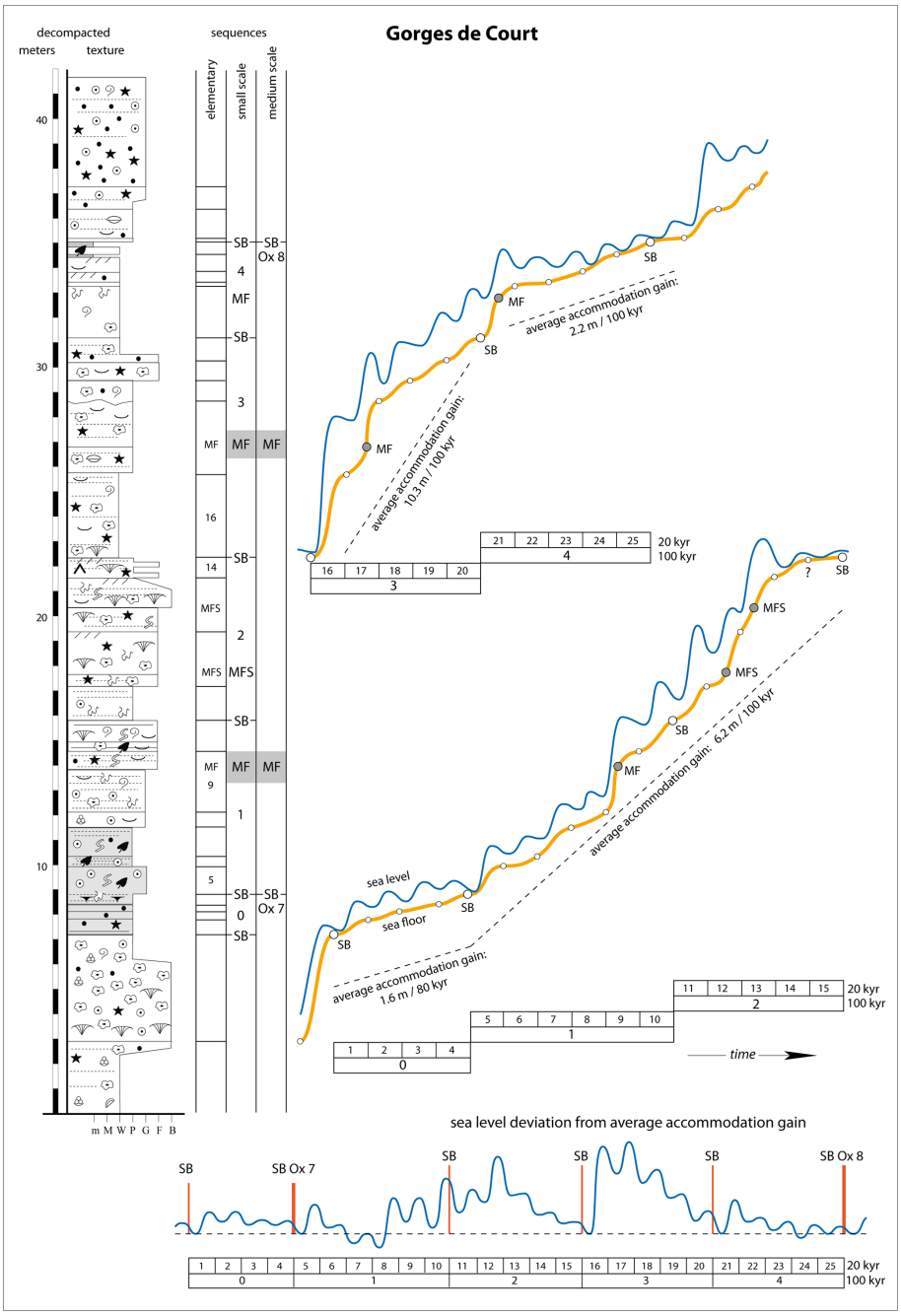

Figure 12. Reconstruction of high-frequency sea level changes for the Gorges de Court section (modified from Strasser, 2018). The section (Fig. 9) is first decompacted according to facies, and for each facies a water depth is attributed. Elementary sequences are assumed to correspond to the 20 kyr precession cycle and small-scale sequences to the 100 kyr one. Average accommodation gain needed to record the small-scale sequences varies through time. By deducing these trends, a sea level curve is reconstructed that serves as input to Fig. 13. Symbols and abbreviations are as in Fig. 7.

process in the case study presented here (Gygi and Persoz, 1986; Hug, 2003).

From Fig. 7 it is clear that the terrigenous material is not recorded equally in the studied sections. This can be explained by the variable platform morphology including highs where the siliciclastics bypassed and lows where they were ponded (e.g. Strasser, 2018). Furthermore, currents picked up the clays and redistributed them over the platform.

At a palaeolatitude of 26 to 27° N (Dercourt et al., 1993), the studied platform was situated in the subtropical zone, which is confirmed by the diversity and type of carbonate-producing organisms typical of such platforms (Reijmer,

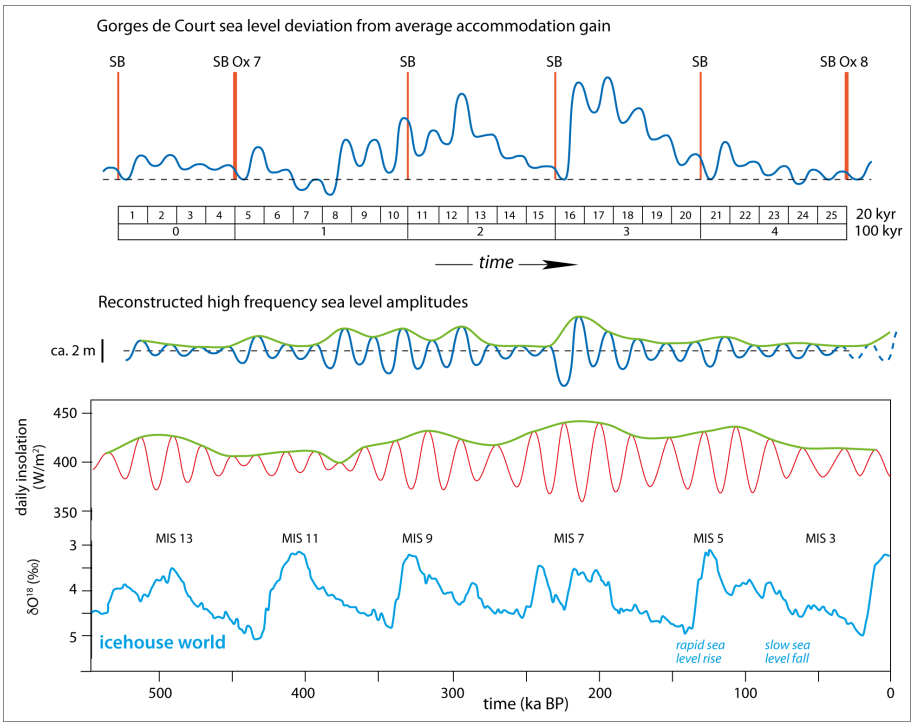

Figure 13. Comparison between the high-frequency, metre-scale sea level changes reconstructed for the Gorges de Court section and the insolation curve calculated for the Equator for the last 550 kyr (Hinnov, 2018). The envelopes of the two curves (green lines) reflect the 100 and 405 kyr eccentricity cycles, suggesting that the sedimentary record at Gorges de Court was at least partly controlled by insolation cycles. During icehouse times, the sea level changes had a much higher amplitude (tens of metres; Shackleton, 1987) and were highly asymmetrical (δ^{18}O values serving as a proxy for sea level changes; simplified from Railsback et al., 2015; MIS: marine isotope stage). For discussion refer to the text.

2021). At this latitude and at the insolation maximum, atmospheric circulation was controlled by the Hadley cell, while at the insolation minimum, the Ferrel cell was active (e.g. Matthews and Perlmutter, 1994). Orbital cyclicity thus caused latitudinal shifts of atmospheric cells and shifts between high-pressure and low-pressure zones. For example, Khon et al. (2012) showed how insolation changes at the 100 kyr scale between the last interglacial (Eemian; MIS 5e) and the early Holocene controlled feedback loops between sea surface temperatures, easterly winds, water evaporation, shifting of the Intertropical Convergence Zone, and circulation patterns of the Hadley and Walker cells. These insolation changes thus indirectly controlled rainfall at a given latitude. Cecca et al. (2005) documented latitudinal shifts of climate belts based on the distribution of coral reefs and ammonites during the Oxfordian. Following the general circulation model developed by Sellwood et al. (2000), they concluded that the late Oxfordian was characterized by low rainfall in the Tethyan Mediterranean area (0.5 to 2 mm per day) and slightly higher rainfall (2 to 4 mm per day) in central and northern Europe.

Orographic effects modifying the atmospheric circulation were probably minor as there was no high mountain range near the Jura platform but only widely dispersed, low-relief massifs (Fig. 5). Insolation minima corresponded to low sea levels (Fig. 13), and this explains why many sequence boundaries in the studied sections contain terrigenous material that was eroded from the hinterland under humid conditions.

More arid conditions prevailed during transgression and maximum flooding, when climate was warmer and sea level rose, allowing for the growth of coral reefs under oligotrophic conditions. However, nutrients were washed into the system, which stimulated microbial growth that eventually smothered the corals, as illustrated in Fig. 10. While corals could still grow at the beginning of the second 20 kyr sequence, they were suffocated by microbialites at the end of this elementary sequence when eutrophication increased. Towards the end of the transgressive part of the small-scale, 100 kyr sequence, eutrophication was such that corals could not grow anymore (Fig. 10). This evolution suggests that nutrients were washed in from the hinterland and affected the reef during transgression and maximum flooding, before the siliciclastics arrived and covered the coral–microbial buildup. The demise of Oxfordian coral reefs in the Swiss Jura due to nutrient and siliciclastic input was documented by Dupraz (1999) and Dupraz and Strasser (2002). Eutrophication can also be caused by increased upwelling bringing nutrients from deep to shallow waters. However, considering

the position of the Jura platform far from the open Tethys ocean (Fig. 5), this scenario is less likely.

Védrine et al. (2007) showed that the morphology of oncoids in the Hauptmumienbank Member varied according to water depth, water energy, and terrigenous nutrient influx; all of these are related to climate changes induced by the 100 and 20 kyr orbital cycles. Analysing coral–microbialite relationships such as those illustrated in Fig. 10, Dupraz (1999) and Dupraz and Strasser (2002) came to the same conclusion. On a ramp at the southern margin of the French Jura platform, Olivier et al. (2011) described abundant microbial carbonates (oncoids and coral–microbialite reefs) that formed during the Bimammatum zone, i.e. during the interval shown in Fig. 7. This they explained by a humid and relatively cool climate, terrigenous nutrient input, and mesotrophic conditions.

On the Aalenian to Oxfordian platform in western France, Andrieu et al. (2016) found that high carbonate productivity correlated with high eccentricity intervals, which promoted a dry climate and oligotrophic conditions for the carbonate-producing organisms. However, they referred to the ca. 9 Myr eccentricity cycle evidenced by Martinez and Dera (2015) in Jurassic to Early Cretaceous Tethyan sections.

A rapid shift from a cool and humid climate to warmer and more arid conditions is recorded in the North Sea at the end of the early Oxfordian (Densiplicatum subzone) and may have been of global extent, related to hydrothermalism at the onset of rifting in the North and South Atlantic (Abbink et al., 2001). From the middle Oxfordian to the Kimmeridgian, the general evolution was towards warmer and more arid conditions (Olivier et al., 2015; Carpentier et al., 2010). However, at the beginning of the late Oxfordian, rainfall increased in the Paris Basin (Brigaud et al., 2014). In the Swiss Jura, this corresponds to the interval around sequence boundary Ox 6 where siliciclastics and terrigenous organic matter are present (Fig. 7). Superimposed on these general trends, rainfall patterns were controlled by the orbital cycles. Above sequence boundary Ox 6, siliciclastics predominate. A well-developed medium-scale sequence controlled by the 405 kyr long eccentricity cycle then leads to sequence boundary zone Ox 7, which again is rich in siliciclastics. Arid conditions are indicated by evaporites in the middle of the next medium-scale sequence (Figs. 7, 9). SB Ox 8 contains only a thin interval of terrigenous material, thus confirming the general trend towards arid conditions in the early Kimmeridgian (Abbink et al., 2001). An interesting issue is the presence of siliciclastics at the maximum flooding of the medium-scale sequences (e.g. at the top of the Steinebach Member at metre 40; Fig. 7). Either there was a pulse of rainfall related to the northward expansion of the Intertropical Convergence Zone (e.g. Khon et al., 2012) or sea level was high enough to reach deep into the land areas and mobilize terrigenous material there.

In the Hautes-Roches and Gorges de Court sections, siliciclastics and plant material are present below sequence boundary Ox 6 (Fig. 7). Marls become important above Ox 6 in all sections shown in the figure, up to the major transgressive surface marking the base of the Steinebach and Hauptmumienbank members. This implies rainfall over the emerged land areas. The same interval also corresponds to the end of the large-scale regressive trend documented in European basins by Hardenbol et al. (1998), meaning that sea level was generally low, that more land was exposed to erosion, and that terrigenous material was forced to prograde into the ocean. More exposed land areas also led to more continental weathering, potentially drawing down atmospheric CO_2 levels. This has been modelled for million-year timescales by e.g. Goddéris et al. (2012), and the feedbacks between weathering and atmospheric CO_2 have also been discussed for future climate change (e.g. Beaulieu et al., 2012). In hemipelagic carbonates in the Jura Mountains and the Vocontian basin, Padden et al. (2002) found negative $\delta^{13}C$ excursions in the Transversarium and Bifurcatus ammonite zones (i.e. below SB Ox 6; Fig. 3), which are explained by the release of methane, introducing light ^{12}C into the marine carbon reservoir. If methane was also released into the atmosphere, it may have contributed to greenhouse effects that led to warming and increased precipitation over the land areas and thus to more siliciclastic input. The general cooling trend due to CO_2 drawdown may thus have been punctuated by short warming periods, but humidity was maintained.

Clay minerals also hold palaeoclimatic information, and the ratio between kaolinite and illite is commonly used to define humid versus arid conditions during soil formation: a high K/I ratio generally indicates a warmer and more humid climate (Curtis, 1990; Thiry, 2000). On the Jura platform, kaolinite becomes dominant over illite above sequence boundary Ox 6 (Gygi and Persoz, 1986). However, rates of soil formation are slow, and the time resolution of the clays deposited in the ocean therefore is considered to be low (1 to 2 Myr; Thiry, 2000). Furthermore, clays may be stored in deltas, ponded in lagoons, and distributed across the platform at different times. Thus, the climate information they contain may not correspond to the time at which they were finally recorded at a given position on the platform. Nevertheless, Védrine (2007) and Strasser et al. (2012) found that in the Hauptmumienbank Member the K/I ratio increases slightly around sequence boundaries and maximum flooding intervals of the small-scale, 100 kyr sequences. At the sequence boundaries, kaolinite is associated with quartz. This implies that the climate was humid during low sea level, and quartz and clays were eroded from the hinterland. At maximum flooding, with the ocean encroaching on the land areas, only clays were mobilized and transported across the platform. As discussed above, there might have also been a humid phase during maximum flooding related to the northward expansion of the Intertropical Convergence Zone.

The importance of the palaeolatitude in the distribution of rainfall patterns is illustrated by the comparison of Oxfor-

dian sequences in the Swiss Jura and in the Soria region of Spain (Pittet and Strasser, 1998). In the small-scale, 100 kyr sequences in the Swiss Jura, siliciclastics are commonly concentrated around the sequence boundaries, while in Spain they occur preferentially in the maximum flooding intervals. The sections studied in Spain were at a palaeolatitude of 23 to 24° N (Dercourt et al., 1993), i.e. 3 to 4° farther south than the Jura sections. This latitudinal difference may explain why the humid periods during a 100 kyr cycle did not occur at the same time.

3.4 Wind and storms

During the Oxfordian, the Jura platform was situated in the subtropical zone and under the influence of trade winds. These would have forced currents into a westerly direction, but the presence of several emergent landmasses certainly deviated these currents. Nevertheless, considering the palaeogeography shown in Fig. 5, it is probable that the siliciclastics found on the Jura platform stemmed mainly from the Bohemian Massif. This massif lies on a more northern palaeolatitude, which implies that rainfall could have increased weathering and erosion there, while on the Jura platform more arid conditions prevailed. This may explain the direct superposition of marly layers on a dolomitized carbonate facies (Fig. 9). Nutrients in a dissolved state travelled faster across the platform and nourished the microbialites before the siliciclastics arrived (Fig. 10).

The cross-bedded ooid and bioclastic shoals encountered in the studied outcrops were mainly controlled by tidal currents, the direction of which varied according to the platform morphology.

Storms episodically affected the platform. Being far away from the open ocean, fetch was reduced. Nevertheless, the presence of reef rubble and washovers (Fig. 10) testifies to currents and waves strong enough to dismantle a reef and throw sediment over topographic highs. As is the case today with global warming, storm frequency and intensity were likely to increase when water temperature increased (Masson-Delmotte et al., 2022). Pittet and Gorin (1997) noted an increase in tempestites and washovers in the marly interval above sequence boundary Ox 6, which corresponds to the highstand of the corresponding 400 kyr sequence (Fig. 7). The abundance of siliciclastics in the interval, however, implies humid conditions and generally low sea level with a cooler climate. Possibly, a preservational bias has to be considered: in very shallow water or in the intertidal zone, only thin layers of sediment are deposited during a storm (for example, on the tidal flats of the Bahamas; Rankey et al., 2004). In deeper water, however, there is room to accommodate the reworked sediment. In the Kimmeridgian of Aquitaine (France), limestone–marl alternations are regularly interrupted by thin tempestite layers (Colombié et al., 2018). It has been shown that tempestite occurrence (and thus storm frequency) was highest during maximum flooding intervals of the sequences controlled by the 405 kyr long eccentricity cycle. Maximum flooding relates to rapid sea level rise forced by a warming of the climate.

3.5 Combined climatic effects at orbital scale

From the discussion above it becomes clear that the sedimentary record of shallow marine carbonate systems is controlled by several interdependent climatic processes. For the Oxfordian in the Swiss Jura, two models are proposed to explain the interactions of climate drivers and the resulting sedimentary record. The shortest decipherable timescale is chosen, i.e. a sea level cycle related to the 20 kyr orbital precession cycle. This approaches the time frame in which Holocene processes took place during the last 10 kyr, and comparisons are thus facilitated. For example, Parkinson (1989) describes a Holocene sedimentary sequence in southwestern Florida where transgression over the Pleistocene substrate started at about 10 ka BP. A first deposit of peat was followed by transgressive coastal marine sediments. As sea level rise decelerated, the turn-around to regressive highstand deposits occurred at 3.5 to 3.2 ka BP, leading to intertidal oyster accumulations and mangrove islands. From 1900 to 2021, however, sea level in southern Florida rose at an average of 2.52 mm yr^{-1}, and from 2000 to 2021 this average was 6.47 mm yr^{-1} (Parkinson and Wdowinski, 2021). Sediment accumulation cannot keep up with this rate, and a transgression occurs. For comparison, the reconstructed Oxfordian rates of the fastest sea level rise are 0.2 to 0.3 mm yr^{-1} (see Sect. 3.2). This recent transgression is due to anthropogenically induced global warming that overrides the orbitally controlled insolation, which has diminished since its peak about 9000 years ago (Fig. 1; Crucifix et al., 2002).

To simplify, the sea level cycle in the models is assumed to have been symmetrical, but asymmetries due to processes mentioned above were certainly present. Accommodation gain is the sum of subsidence and long-term sea level rise. Subsidence in the Late Jurassic of the Jura platform was about 3 m per 100 kyr (Wildi et al., 1989). Long-term sea level rise is taken from the example in Fig. 12: 405 kyr to accumulate 26 m of decompacted sediment up to the tidal flat at sequence boundary Ox 8 (Fig. 9) results in 6.4 m per 100 kyr of total accommodation gain. This value minus the subsidence gives 3.4 m per 100 kyr long-term sea level rise. This is consistent with the major transgressive evolution in European basins from the Oxfordian to the Kimmeridgian, which started in the Semimammatum subzone with the major transgressive surface above sequence boundary Ox 6 (Hardenbol et al., 1998).

Two hypothetical models for the formation of depositional sequences are presented in Fig. 14. Model (a) (inspired from the middle part of the detailed Gorges de Court section; Fig. 9) describes the formation of an elementary sequence controlled by the 20 kyr precession cycle. This cycle is situated in the middle of a 100 kyr and/or 405 kyr cycle when

insolation was high (Fig. 1). It is thus expected that sea level amplitudes on the 20 kyr scale were relatively high: of the order of a few metres (Figs. 12, 13). For the model, an amplitude of 3 m is chosen, and it is assumed that the base and top of the elementary sequence are at zero sea level. At the beginning of the cycle, the climate at the given subtropical latitude is humid, sea level is low, and siliciclastics are eroded from the emergent massifs, transported across the platform, and accumulated at the base of the sequence. Accommodation is low, and only a thin sediment layer can be recorded. With increasing insolation, the climate becomes progressively dry, the water becomes warmer and expands to rise sea level, coastlines retreat, rivers are less active, and siliciclastic input is reduced. At still low sea level, a tidal flat forms and can keep up for a while with rising sea level before it is drowned. With increasing water depth, conditions become ideal for carbonate production, and high accommodation gives room for the accumulation of ooid shoals and the growth of coral reefs. Of course, depending on the position on the platform, lateral facies variations are considerable: while at one point reef growth can keep up with rising sea level, at another point a deep lagoon develops (Fig. 2). The demise of the hypothetical coral reef could be due to eutrophication like in the example of Fig. 10 or to smothering by sediment that progrades because sea level rise slows down. Still under a warm and arid climate, sea level rise slows down and allows the sediment to fill in the available space. If sea level then drops below the sediment surface and the climate becomes humid again, a karst develops. If the sediment surface stays in the intertidal or supratidal zone as in Fig. 14a, evaporites form in a sabkha under an arid climate. When insolation decreases in the second part of the 20 kyr cycle, climate at this given latitude becomes cooler and more humid, and the cycle starts over again. It is clear from Fig. 14a that the time interval of vigorous sedimentation covers only a short part of the 20 000 years and that much time is represented by the sequence boundaries (e.g. Strasser, 2015).

Model (b) (inspired from the Ox 7 sequence boundary zone at Gorges de Court; Fig. 9) illustrates the situation during generally low insolation at the 100 kyr and/or 405 kyr scale (Fig. 1). Sea level amplitudes at the 20 kyr scale are low (Fig. 13), and an amplitude of 1 m is chosen for the model. The climate is rather cool and humid. Consequently, more land areas are exposed, rainfall favours their erosion, rivers are active, and deltas prograde. Consequently, the elementary sequence will be dominated by siliciclastics. A relatively short time interval of less humid conditions and warmer temperatures allows for some carbonate production, but siliciclastics are still present. Again, much time of this cycle is spent in intertidal to supratidal conditions.

From the graphs in Fig. 14 (representing decompacted sediment) sedimentation rates can be deduced. At the fastest accumulation on the seafloor during about 2000 years (corresponding to the fastest rise of sea level) about 1 m of coral reef is built in model (a). This results in a sedimentation rate of 0.5 mm yr^{-1}. In model (b), representing a siliciclastic-dominated scenario, only 30 cm of lagoonal facies accumulate in 2000 years, giving a sedimentation rate of 0.15 mm yr^{-1}. Holocene rates for these environments reach 14 mm yr^{-1} for a healthy reef and between 1 and 2 mm yr^{-1} for a tidal flat (Enos, 1991; Strasser and Samankassou, 2003). This discrepancy does not necessarily imply that sedimentation rates in the Oxfordian were generally lower than in the Holocene but rather that the time of non-deposition, reworking, and/or condensation is underestimated in the models (Sadler, 1994; Strasser, 2015).

These two models must undergo many modifications depending on the position on the platform, the currents distributing nutrients and siliciclastics, and the ecology of the carbonate-producing organisms. Also, they are idealized cases in which facies evolution exhibits deepening–shallowing trends within an elementary sequence. In the studied sections, this is not always the case, and facies may stay the same throughout the sequence (with the exception of the marly layers at the sequence boundaries). This may be due to bioturbation that homogenized the sediment in a lagoon or to constant reworking by waves and currents in the case of an ooid shoal. Nevertheless, the models illustrate the potential of shallow marine carbonates to record climate changes at a relatively high time resolution.

4 Conclusions

Orbital cycles controlling the energy received by the Earth from the sun are important drivers of environmental changes that occur on land and in the ocean. In the case study presented here, it is shown that, during the Oxfordian (Late Jurassic), the shallow marine carbonate systems on the platform of the Swiss Jura Mountains reacted to these changes at the frequencies of the long and short eccentricity cycles (405 and 100 kyr, respectively) as well as the precession cycle (20 kyr in the Oxfordian). The main controlling factors were metre-scale sea level changes and climate changes between humid and arid. Insolation changes translated more or less directly into eustatic sea level changes through thermal expansion and retraction of the ocean surface waters. In addition, glacioeustasy and aquifer eustasy certainly occurred but are difficult to quantify. At all frequencies, humid and cool periods corresponded to low insolation and low sea level, while arid and warm periods prevailed during intervals of high insolation and high sea level. At a subtropical latitude on the shallow marine platform, many carbonate-producing organisms (e.g. algae, foraminifera, gastropods, bivalves, serpulids) were present, and coral reefs were especially sensitive to environmental changes. Ooids, oncoids, and microbialites also contributed to the sediment.

An interval of 1.2 Myr is discussed, calibrated by biostratigraphy, chronostratigraphy, and sequence stratigraphy. Three detailed sections are chosen to illustrate the evo-

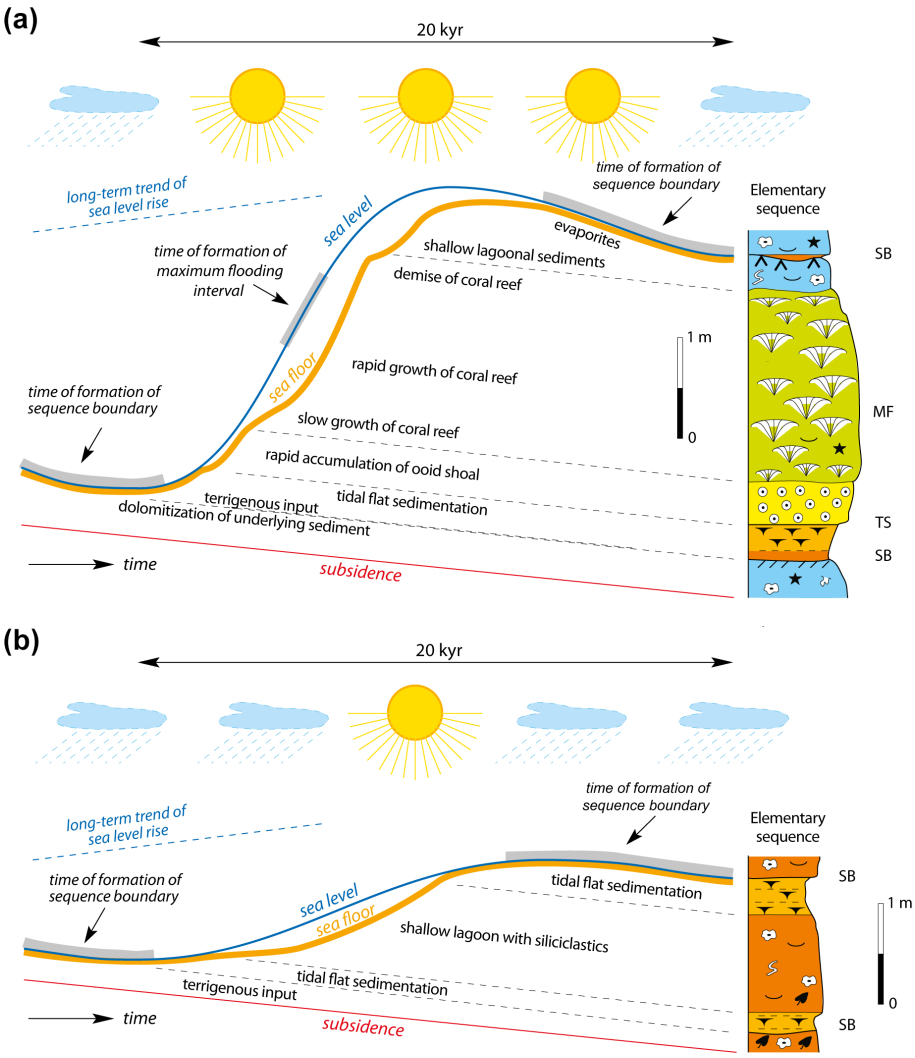

Figure 14. Conceptual models that explain the formation of elementary sequences as a function of climate changes in tune with the orbital precession cycle. **(a)**: high insolation within a 100 and/or 405 kyr eccentricity cycle; **(b)**: low insolation. For discussion refer to the text. Symbols and abbreviations are as in Fig. 7.

lution of the facies and stacking pattern of the depositional sequences within this interval. During high insolation in the middle of a 405 kyr cycle, high amplitudes of sea level fluctuations and arid conditions allowed for the development of ooid shoals and coral reefs. However, the corals were regularly encrusted by microbialites, suggesting nutrient input even under an arid climate. At low insolation, low sea level amplitudes, and more humid and cooler conditions, siliciclastics were washed into the system and hampered the organic carbonate production.

The orbital frequencies are reflected in the hierarchical stacking of sequences: medium- and small-scale sequences formed in tune with the 405 and 100 kyr eccentricity cycles, respectively, while the 20 kyr precession cycles controlled the formation of elementary sequences. The obliquity cycle was not detected in the studied outcrops. After decompaction of the sections and estimation of the water depths in which the different facies evolved, a composite sea level curve has been reconstructed. It compares well with the curve of insolation changes over the last 550 kyr.

Based on the studied sections and the facies encountered, two models are presented. Model (a) describes the growth and demise of a coral reef in warm waters and a high-amplitude sea level rise to accommodate the reef. Arid conditions are exemplified by evaporites. Model (b) simulates a low-amplitude sea level cycle and rainfall in the hinterland that washed siliciclastics and plant matter onto the platform. The sedimentation rates deduced from the models are below those of Holocene sedimentary environments, implying that the time of non-deposition in the models is probably underestimated.

Despite the high lateral and vertical facies variability on the Oxfordian carbonate platform, despite the uncertainties in attributing water depth and compaction factors to the different facies, and despite the multiple feedback loops between insolation at the top of the atmosphere and the depositional environment, this study demonstrates the potential of shallow marine carbonates to record climate changes at the frequencies of orbital cycles. The time resolution of 20 000 years (the precession cycle) offers the opportunity to estimate rates of sea level change, ecological processes, and sediment accumulation in the geologic past. The interpretation of the evolution of ancient sedimentary systems can thus be refined and better compared to today's changes in ecosystems. Concerning the rate of climate change, this study implies that anthropogenically induced global warming and subsequent sea level rise today are occurring more than 10 times faster than the fastest rise reconstructed for the Oxfordian.

Data availability. All data are published in the cited papers and theses.

Competing interests. The author has declared that there are no competing interests.

Disclaimer. Publisher's note: Copernicus Publications remains neutral with regard to jurisdictional claims in published maps and institutional affiliations.

Acknowledgements. I thank the editor Denis-Didier Rousseau for having invited me to write this contribution. It is based on fieldwork and research carried out by many MSc and PhD students at the University of Fribourg and was financed mainly by the Swiss National Science Foundation. Their intellectual, institutional, and financial support is gratefully acknowledged. I also thank the reviewers Simon Andrieu and Marc Aurell, whose constructive comments greatly improved the paper.

Financial support. I acknowledge the funding by the Swiss National Science Foundation (grant nos. 20-41888, 20-43150, 20-46625, 20-56491, 20-67736, 20-109214).

Review statement. This paper was edited by Denis-Didier Rousseau and reviewed by Marc Aurell and Simon Andrieu.

References

Abbink, O., Targarona, J., Brinkhuis, H., and Visscher, H.: Late Jurassic to earliest Cretaceous palaeoclimatic evolution of the southern North Sea, Global Planet. Change, 30, 231–256, https://doi.org/10.1016/S0921-8181(01)00101-1, 2001.

Allenbach, R. P.: Synsedimentary tectonics in an epicontinental sea: a new interpretation of the Oxfordian basins of northern Switzerland, Eclogae Geol. Helv., 94, 265–287, 2001.

Andrieu, S., Brigaud, B., Barbarand, J., Lasseur, E., and Saucède, T.: Disentangling the control of tectonics, eustasy, trophic conditions and climate on shallow-marine carbonate production during the Aalenian–Oxfordian interval: From the western France platform to the western Tethyan domain, Sed. Geol., 345, 54–84, https://doi.org/10.1016/j.sedgeo.2016.09.005, 2016.

Amies, J. D., Rohling, E. J., Grant, K. M., Rodriguez-Sanz, L., and Marino, G.: Quantification of African monsoon runoff during last interglacial sapropel S5, Paleoceanogr. Paleoclim., 34, 1487–1516, https://doi.org/10.1029/2019PA003652, 2019.

Anderson, T. F. and Arthur, M. A.: Stable isotopes of oxygen and carbon and their application to sedimentology and paleoenvironmental problems, SEPM Short Course, 10, 151 p., 1983.

Armstrong, H. A., Wagner, T., Herrinshaw, L. G., Farnsworth, A. J., Lunt, D. J., Harland, M., Imber, J., Loptson, C., and Atar, E. F. L.: Hadley circulation and precipitation changes controlling black shale deposition in the Late Jurassic Boreal Seaway, Paleoceanography, 31, 1041–1053, https://doi.org/10.1002/2015PA002911, 2016.

Beaulieu, E., Goddéris, Y., Donnadieu, Y., Labat, D., and Roelandt, C.: High sensitivity of the continental-weathering carbon dioxide sink to future climate change, Nat. Clim. Change, 2, 346–349, https://doi.org/10.1038/NCLIMATE1419, 2012.

Berger, A., Loutre, M.-F., and Laskar, J.: Stability of the astronomical frequencies over the Earth's history for paleoclimatic studies, Science, 255, 560–566, https://doi.org/10.1126/science.255.5044.560, 1992.

Berggren, W. A., Kent, D. V., Aubry, M. P., and Hardenbol, J. (Eds.): Geochronology, Time Scales and Global Stratigraphic Correlation, SEPM Spec. Publ., 54, 386 pp., 1995.

Boulila, S., Galbrun, B., Hinnov, L. A., Collin, P.-Y., Ogg, J. G., Fortwengler, D., and Marchand, D.: Milankovitch and sub-Milankovitch forcing of the Oxfordian (Late Jurassic) Terres Noires Formation (SE France) and global implications, Basin Res., 22, 717–732, https://doi.org/10.1111/j.1365-2117.2009.00429.x, 2010.

Brigaud, B., Vincent, B., Carpentier, C., Robin, C., Guillocheau, F., Yven, B., and Huret, E.: Growth and demise of the Jurassic carbonate platform in the intracratonic Paris Basin (France): Interplay of climate change, eustasy and tectonics, Marine Petrol. Geol., 53, 3–29, https://doi.org/10.1016/j.marpetgeo.2013.09.008, 2014.

Carpentier, C., Lathuilière, B., and Ferry, S.: Sequential and climatic framework of the growth and demise of a carbonate platform: implications for the peritidal cycles (Late Jurassic, north-eastern France), Sedimentology, 57, 985–1020, https://doi.org/10.1111/j.1365-3091.2009.01128.x, 2010.

Carpentier, C., Martin-Garin, B., Lathuilière, B., and Ferry, S.: Correlation of reefal Oxfordian episodes and climatic implications in the eastern Paris Basin (France), Terra Nova, 18, 191–201, https://doi.org/10.1111/j.1365-3121.2006.00679.x, 2006.

Catuneanu, O., Abreu, V., Bhattacharya J. P., Blum, M. D, Dalrymple, R. W., Eriksson, P. G., Fielding, C. R., Fisher, W. L., Galloway, W. E., Gibling, M. R., Giles, K. A., Holbrook, J. M.,

Jordan, R., Kendall, C. G. St. C., Macurda, B., Martinsen, O. J., Miall, A. D., Neal, J. E., Nummedal, D., Pomar L., Posamentier H. W., Pratt, B. R., Sarg, J. F., Shanley, K. W., Steel, R. J., Strasser, A., Tucker, M. E., and Winker, C.: Towards the standardization of sequence stratigraphy, Earth-Sci. Rev., 92, 1–33, https://doi.org/10.1016/j.earscirev.2008.10.003, 2009.

Cecca, F., Martin-Garin, B., Marchand, D., Lathuilière, B., and Bartolini, A.: Paleoclimatic control of biogeographic and sedimentary events in Tethyan and peri-Tethyan areas during the Oxfordian (Late Jurassic), Palaeogeo., Palaeoclim., Palaeoecol., 222, 10–32, https://doi.org/10.1016/j.palaeo.2005.03.009, 2005.

Church, J. A. and Clark, P. U. (coordinating lead authors): Sea Level Change, in: Climate Change 2013: The Physical Science Basis. Contribution of Working Group I to the Fifth Assessment Report of the Intergovernmental Panel on Climate Change, Cambridge Univ. Press, 1137–1216, 2013.

Colombié, C., Carcel, D., Lécuyer, C., Ruffel, A., and Schnyder, J.: Temperature and cyclone frequency in Kimmeridgian Greenhouse period (late Jurassic), Global Planet. Change, 170, 126–145, https://doi.org/10.1016/j.gloplacha.2018.08.005, 2018.

Colombié, C., Lécuyer, C., and Strasser, A.: Carbon- and oxygen-isotope records of palaeoenvironmental and carbonate production changes in shallow-marine carbonates (Kimmeridgian, Swiss Jura), Geol. Mag., 148, 133–153, https://doi.org/10.1017/S0016756810000518, 2011.

Crucifix, M., Loutre, M.-F., Tulkens, P., Fichefet, T., and Berger, A. : Climate evolution during the Holocene: a study with an Earth system model of intermediate complexity, Clim. Dynam., 19, 43–60, https://doi.org/10.1007/s00382-001-0208-6, 2002.

Curtis, C. D.: Aspects of climate influence on the clay mineralogy and geochemistry of soils, paleosols and clastic sedimentary rocks, J. Geol. Soc. London, 147, 351–357, https://doi.org/10.1144/gsjgs.147.2.0351, 1990.

Davies, A., Gréselle, B., Hunter, S. J., Baines, G., Robson, C., Haywood, A., David C. Ray, D. C., Simmons, M. D., and van Buchem, F. S. P.: Assessing the impact of aquifer-eustasy on short-term Cretaceous sea-level, Cretaceous Res., 112, 104445, https://doi.org/10.1016/j.cretres.2020.104445, 2020.

Dercourt, J., Ricou, L. E., and Vrielynck, B. (Eds): Atlas: Tethys Palaeoenvironmental Maps, Gauthier-Villars, Paris, 1993.

de Winter, N. J., Zeeden, C., and Hilgen, F. J.: Low-latitude climate variability in the Heinrich frequency band of the Late Cretaceous greenhouse world, Clim. Past, 10, 1001–1015, https://doi.org/10.5194/cp-10-1001-2014, 2014.

Dunham, R. J.: Classification of carbonate rocks according to depositional texture, AAPG Mem., 1, 108–121, 1962.

Dupraz, C.: Paléontologie, paléoecologie et évolution des faciès récifaux de l'Oxfordien moyen-supérieur (Jura suisse et français), Ph.D. thesis, GeoFocus, 2, Fribourg, Switzerland, 247 pp., 1999.

Dupraz, C. and Strasser, A.: Nutritional modes in coral-microbialite reefs (Jurassic, Oxfordian, Switzerland): evolution of trophic structure as a response to environmental change, Palaios, 17, 449–471, https://doi.org/10.1669/0883-1351(2002)017<0449:NMICMR>2.0.CO;2, 2002.

Embry, A. F. and Klovan, J. E.: A late Devonian reef tract on northeastern Banks Island, N.W.T., Bull. Canadian Petrol. Geol., 19, 730–781, 1971.

Enos, P.: Sedimentary parameters for computer modeling, Kansas Geol. Survey Bull., 233, 63–99, 1991.

Feng, R. and Poulsen, C. J.: Andean elevation control on tropical Pacific climate and ENSO, Paleoceanography, 29, 795–809, https://doi.org/10.1002/2014PA002640, 2014.

Flügel, E.: Microfacies of Carbonate Rocks, Springer, Berlin, Germany, 976 pp., ISBN 354022016X, 2004.

Frakes, L. A., Francis, J. E., and Syktus, J. I.: Climate Modes of the Phanerozoic, Cambridge Univ. Press, 274 pp., 1992.

Goddéris, Y., Donnadieu, Y., Lefebvre, V., Le Hir, G., and Nardin, E..: Tectonic control of continental weathering, atmospheric CO_2, and climate over Phanerozoic times, C. R. Geoscience, 344, 652–662, https://doi.org/10.1016/j.crte.2012.08.009, 2012.

Goldhammer, R. K.: Compaction and decompaction algorithms for sedimentary carbonates, J. Sed. Res., 67, 26–35, https://doi.org/10.1306/D42684E1-2B26-11D7-8648000102C1865D, 1997.

Gradstein, F. M., Ogg, J. G., Schmitz, M. D., and Ogg, G. (Eds.): Geologic Time Scale 2020, Vol. 1, Elsevier, Amsterdam, The Netherlands, 1357 pp., 2020.

Gygi, R. A.: Datierung von Seichtwassersedimenten des Späten Jura in der Nordwestschweiz mit Ammoniten, Eclogae Geol. Helv., 88, 1–58, 1995.

Gygi, R. A.: Integrated stratigraphy of the Oxfordian and Kimmeridgian (Late Jurassic) in northern Switzerland and adjacent southern Germany, Mem. Swiss Acad. Sci., 104, 152 pp., 2000.

Gygi, R. A. and Persoz, F.: Mineralostratigraphy, litho- and biostratigraphy combined in correlation of the Oxfordian (Late Jurassic) formations of the Swiss Jura range, Eclogae Geol. Helv., 79, 385–454, 1986.

Gygi, R. A., Coe, A. L., and Vail, P. R.: Sequence stratigraphy of the Oxfordian and Kimmeridgian stages (Late Jurassic) in northern Switzerland, SEPM Spec. Publ., 60, 527–544, 1998.

Hallock, P. and Schlager, W.: Nutrient excess and the demise of coral reefs and carbonate platforms, Palaios, 1, 389–398, 1986.

Hardenbol, J., Thierry, J., Farley, M. B., Jacquin, T., de Graciansky, P.-C., and Vail, P. R.: Jurassic sequence chronostratigraphy, in: Mesozoic and Cenozoic Sequence Stratigraphy of European Basins, edited by: de Graciansky, P.-C., Hardenbol, J., Jacquin, T., and Vail, P. R, SEPM Spec. Publ., 60, 1998.

Hesselbo, S. P., Ogg, J. G., and Ruhl, M.: The Jurassic Period, in: Geologic Time Scale 2020, vol. 1, edited by: Gradstein, F. M., Ogg, J. G., Schmitz, M. D., and Ogg, G., Elsevier, Amsterdam, The Netherlands, 955–1021, 2020.

Hinnov, L. A.: Cyclostratigraphy and astrochronology in 2018, in: Stratigraphy and Timescales, vol. 3, edited by: Montenari, M., Elsevier, Amsterdam, The Netherlands, 1–80, https://doi.org/10.1016/bs.sats.2018.08.004, 2018.

Huang, C.: Astronomical time scale for the Mesozoic, in: Stratigraphy and Timescales, vol. 3, edited by: Montenari, M., Elsevier, Amsterdam, The Netherlands, 81–150, https://doi.org/10.1016/bs.sats.2018.08.005, 2018.

Hug, W.: Sequenzielle Faziesentwicklung der Karbonatplattform des Schweizer Jura im späten Oxford und frühesten Kimmeridge, Ph.D. thesis, GeoFocus 7, Univ. Fribourg, Switzerland, 156 pp., 2003.

Ikeda, M., Ozaki, K., and Legrand, J.: Impact of 10-Myr scale monsoon dynamics on Mesozoic climate and ecosystems, Nat. Sci. Rep., 10, 11984, https://doi.org/10.1038/s41598-020-68542-w, 2020.

Immenhauser, A., Della Porta, G., Kenter, J. A. M., and Bahamonde, J. R.: An alternative model for positive shifts in shallow-marine carbonate δ^{13}C and δ^{18}O, Sedimentology, 50, 953–959, https://doi.org/10.1046/j.1365-3091.2003.00590.x, 2003.

Jacobs, D. K. and Sahagian, D. L.: Climate-induced fluctuations in sea level during non-glacial times, Nature, 361, 710–712, https://doi.org/10.1038/361710a0, 1993.

Jordan, P.: Géologie de la région de Montoz (Jura bernois) avec analyse séquentielle de deux profiles de l'Oxfordien moyen et supérieur. Unpubl. diploma thesis, Univ. Fribourg, Switzerland, 104 pp., 1999.

Khon, V. C., Park, W., Latif, M., Mokhov, I. I., and Schneider, B.: Tropical circulation and hydrological cycle response to orbital forcing, Geophys. Res. Lett., 39, L15708, https://doi.org/10.1029/2012GL052482, 2012.

Laskar, J., Fienga, A., Gastineau, M., and Manche, H.: La2010: a new orbital solution for the long term motion of the Earth, Astron. Astrophys., 532, A89, https://doi.org/10.1051/0004-6361/201116836, 2011.

Laurin, J., Meyers, S. R., Uličnyì, D., Jarvis, I., and Sageman, B. B.: Axial obliquity control on the greenhouse carbon budget through middle- to high-latitude reservoirs, Paleoceanography, 30, 133–149, https://doi.org/10.1002/2014PA002736, 2015.

Lefort, A., Lathuilière, B., Carpentier, C., and Huault, V.: Microfossil assemblages and relative sea-level fluctuations in a lagoon at the Oxfordian/Kimmeridgian boundary (Upper Jurassic) in the eastern part of the Paris Basin, Facies, 57, 649–662, https://doi.org/10.1007/s10347-010-0259-4, 2011.

Leinfelder, R. R., Schmid, D. U., Nose, M., and Werner, W.: Jurassic reef patterns – the expression of a changing globe, SEPM Spec. Publ., 72, 465–520, 2002.

Louis-Schmid, B., Rais, P., Schaeffer, P., Bernasconi, S. M., and Weissert, H.: Plate tectonic trigger of changes in pCO_2 and climate in the Oxfordian (Late Jurassic): Carbon isotope and modeling evidence, Earth Planet. Sci. Lett., 258, 44–60, https://doi.org/10.1016/j.epsl.2007.03.014, 2007.

Lourens, L. J., Hilgen, F. J., Raffi, I., and Vergnaud-Grazzini, C.: Early Pleistocene chronology of the Vrica Section (Calabria, Italy), Paleoceanography, 11, 797–812, https://doi.org/10.1029/96PA02691, 1996.

Martin-Garin, B., Lathuilière, B., Geister, J., and Ramseyer, K.: Oxygen isotopes and climatic control of Oxfordian coral reefs (Jurassic, Tethys), Palaios, 25, 721–729, https://doi.org/10.2110/palo.2010.p10-027r, 2010.

Martinez, M.: Mechanisms of preservation of the eccentricity and longer-term Milankovitch cycles in detrital supply and carbonate production in hemipelagic marl-limestone alternations, in: Stratigraphy and Timescales, vol. 3, edited by: Montenari, M., Elsevier, Amsterdam, The Netherlands, 189–218, https://doi.org/10.1016/bs.sats.2018.08.002, 2018.

Martinez, M. and Dera, G.: Orbital pacing of carbon fluxes by a $\sim$9-My eccentricity cycle during the Mesozoic, P. Natl. Acad. Sci. USA, 112, 12604–12609, https://doi.org/10.1073/pnas.1419946112, 2015.

Masson-Delmotte, V., Zhai, P., Pirani, A., Connors, S. L., Péan, C., Berger, S., Caud, N., Chen, Y., Goldfarb, L., Gomis, M. I., Huang, M., Leitzell, K., Lonnoy, E., Matthews, J. B. R., Maycock, T. K., Waterfield, T., Yelekçi, O., Yu, R., and B. Zhou, B. (Eds.): Climate Change 2021: The Physical Science Basis. Contribution of Working Group I to the Sixth Assessment Report of the Intergovernmental Panel on Climate Change, Cambridge Univ. Press, 2022.

Matthews, M. D. and Perlmutter, M. A.: Global cyclostratigraphy: an application to the Eocene Green River basin, in: Orbital Forcing and Cyclic Sequences, edited by: de Boer, P. and Smith, D. G., IAS Spec. Publ., 19, 459–481, 1994.

Mitchum Jr., R. M. and Van Wagoner, J. C.: High-frequency sequences and their stacking patterns: sequence-stratigraphic evidence of high-frequency eustatic cycles, Sed. Geol., 70, 131–160, https://doi.org/10.1016/0037-0738(91)90139-5, 1991.

Montañez, I. A. and Osleger, D. A.: Parasequence stacking patterns, third-order accommodation events, and sequence stratigraphy of Middle to Upper Cambrian platform carbonates, Bonanza King Formation, southern Great Basin, AAPG Mem., 57, 305–326, 1993.

Ogg, J. G., Hinnov, L. A., and Huang, C.: Jurassic, in: The Geologic Time Scale 2012, edited by: Gradstein, F. M., Ogg, J. G., Schmitz, M. D., and Ogg, G., Elsevier, Amsterdam, The Netherlands, 731–791, 2012.

Ogg, J. G., Ogg, G., and Gradstein, F.: A Concise Geologic Time Scale 2016, Elsevier, Amsterdam, The Netherlands, 234 pp., ISBN 978-0-444-63771-0, 2016.

Olivier, N., Cariou, E., and Hantzpergue, P.: Evolution of a late Oxfordian – early Kimmeridgian carbonate platform, French Jura Mountains, Swiss J. Geosci., 108, 273–288, https://doi.org/10.1007/s00015-015-0189-9, 2015.

Olivier, N., Colombié, C., Pittet, B., and Lathuilière, B.: Microbial carbonates and corals on the marginal French Jura platform (Late Oxfordian, Molinges section), Facies, 57, 469–492, https://doi.org/10.1007/s10347-010-0246-9, 2011.

Padden, M., Weissert, H., Funk, H., Schneider, S., and Gansner, C.: Late Jurassic lithological evolution and carbon-isotope stratigraphy of the western Tethys, Eclogae geol. Helv., 95, 333–346, 2002.

Parkinson, R. W.: Decelerating Holocene sea-level rise and its influence on Southwest Florida coastal evolution: a transgressive/regressive stratigraphy, J. Sed. Petrol., 59, 960–972, 1989.

Parkinson, R. W. and Wdowinski, S.: Accelerating sea level rise and the fate of South Florida coastal wetlands, SSRN, https://doi.org/10.2139/ssrn.3967429, 2021.

Pittet, B.: Contrôles climatiques, eustatiques et tectoniques sur des systèmes mixtes carbonates-siliciclastiques de plate-forme: exemples de l'Oxfordien (Jura suisse, Normandie, Espagne), Ph.D. thesis, Univ. Fribourg, Switzerland, 258 pp., 1996.

Pittet, B. and Gorin, G. E.: Distribution of sedimentary organic matter in a carbonate-siliciclastic platform environment: Oxfordian in the Swiss Jura Mountains, Sedimentology, 44, 915–937, https://doi.org/10.1046/j.1365-3091.1997.d01-58.x, 1997.

Pittet, B. and Strasser, A.: Long-distance correlations by sequence stratigraphy and cyclostratigraphy: examples and implications (Oxfordian from the Swiss Jura, Spain, and Normandy), Geol. Rundsch., 86, 852–874, https://doi.org/10.1007/s005310050181, 1998.

Plunkett, J. M.: Early Diagenesis of shallow platform carbonates in the Oxfordian of the Swiss Jura Mountains, PhD thesis, Univ. Fribourg, Switzerland, 155 pp., 1997.

Pratt, B. R. and James, N. P.: The St George Group (Lower Ordovician) of western Newfoundland: tidal flat is-

land model for carbonate sedimentation in shallow epeiric seas, Sedimentology, 33, 313–343, https://doi.org/10.1111/j.1365-3091.1986.tb00540.x, 1986.

Railsback, L. B., Gibbard, P. L., Head, M. J., Voarintsoa, N. R. G., and Toucanne, S.: An optimized scheme of lettered marine isotope substages for the last 1.0 million years, and the climatostratigraphic nature of isotope stages and substages, Quaternary Sci. Rev., 111, 94–106, https://doi.org/10.1016/j.quascirev.2015.01.012, 2015.

Rais, P., Louis-Schmid, B., Bernasconi, S. M., and Weissert, H.: Palaeoceanographic and palaeoclimatic reorganization around the Middle-Late Jurassic transition, Palaeogeo., Palaeoclim., Palaeoeco., 251, 527–546, https://doi.org/10.1016/j.palaeo.2007.05.008, 2007.

Rankey, E. C. and Reeder, S. L .: Controls on platform-scale patterns of surface sediments, shallow Holocene platforms. Bahamas, Sedimentology, 57, 1545–1565, https://doi.org/10.1111/j.1365-3091.2010.01155.x, 2010.

Rankey, E. C., Enos, P., Steffen, K., and Druke, D.: Lack of impact of Hurricane Michelle on tidal flats, Andros Island, Bahamas: Integrated remote sensing and field observations, J. Sed. Res., 74, 654–661, https://doi.org/10.1306/021704740654, 2004.

Ray, D. C., van Buchem, F. S. P., Baines, G., Davies, A., Gréselle, B., Simmons, M. D., and Robson, C.: The magnitude and cause of short-term eustatic Cretaceous sea-level change: a synthesis, Earth-Sci. Rev., 197, 102901, https://doi.org/10.1016/j.earscirev.2019.102901, 2019.

Reijmer, J. J. G.: Marine carbonate factories: review and update, Sedimentology, 68, 1729–1796, https://doi.org/10.1111/sed.12878, 2021.

Sadler, P. M.: The expected duration of upward-shallowing peritidal carbonate cycles and their terminal hiatuses, Bull. Geol. Soc. Am., 106, 791–802, https://doi.org/10.1130/0016-7606(1994)106<0791:TEDOUS>2.3.CO;2, 1994.

Sames, B., Wagreich, M., Wendler, J. E., Haq, B. U., Conrad, C. P., Melinte-Dobrinescu, M. C., Hu, X., Wendler, I., Wolfgring, E., Yilmaz, I., and Zorina, S. O.: Review: Short-term sea-level changes in a greenhouse world – a view from the Cretaceous, Palaeogeo. Palaeoclim., Palaeoeco., 441, 393–411, https://doi.org/10.1016/j.palaeo.2015.10.045, 2016.

Schoepf, V., Falter, J. L., and McCulloch, M. T.: Limits to the thermal tolerance of corals adapted to a highly fluctuating, naturally extreme temperature environment, Sci. Rep., 5, 17639, https://doi.org/10.1038/srep17639, 2015.

Schulz, M. and Schäfer-Neth, C.: Translating Milankovitch climate forcing into eustatic fluctuations via thermal deep water expansion: a conceptual link, Terra Nova, 9, 228–231, https://doi.org/10.1111/j.1365-3121.1997.tb00018.x, 1997.

Shackleton, N. J.: Oxygen isotopes, ice volume and sea level, Quaternary Sci. Rev., 6, 183–190, https://doi.org/10.1016/0277-3791(87)90003-5, 1987.

Sellwood, B. W. and Valdes, P. J.: Jurassic climates, Proc. Geol. Assoc., 119, 5–17, https://doi.org/10.1016/S0016-7878(59)80068-7, 2008.

Sellwood, B. W., Valdes, P. J., and Price, G. D.: Geological evaluation of multiple general circulation model simulations of Late Jurassic palaeoclimate, Palaeogeo. Palaeoclim. Palaeoeco., 156, 147–160, https://doi.org/10.1016/S0031-0182(99)00138-8, 2000.

Stienne, N.: Paléoécologie et taphonomie comparative en milieux carbonatés peu profonds (Oxfordien du Jura suisse et Holocène du Belize), Ph.D. thesis, GeoFocus, 22, Univ. Fribourg, Switzerland, 248 pp., 2010.

Strasser, A.: Lagoonal-peritidal sequences in carbonate environments: autocyclic and allocyclic processes, in: Cycles and Events in Stratigraphy, edited by: Einsele, G., Ricken, W., and Seilacher, A., Springer, Heidelberg, Germany, 709–721, 1991.

Strasser, A.: Astronomical time scale for the Middle Oxfordian to Late Kimmeridgian in the Swiss and French Jura Mountains, Swiss J. Geosci., 100, 407–429, https://doi.org/10.1007/s00015-007-1230-4, 2007.

Strasser, A.: Hiatuses and condensation: an estimation of time lost on a shallow carbonate platform, Depositional Record, 1, 91–117, https://doi.org/10.1002/dep2.9, 2015.

Strasser, A.: Cyclostratigraphy of shallow-marine carbonates – limitations and opportunities, in: Stratigraphy and Timescales, vol. 3, edited by: Montenari, M., Elsevier, Amsterdam, The Netherlands, 151–187, https://doi.org/10.1016/bs.sats.2018.07.001, 2018.

Strasser, A. and Samankassou, E.: Carbonate sedimentation rates today and in the past: Holocene of Florida Bay, Bahamas, and Bermuda vs. Upper Jurassic and Lower Cretaceous of the Jura Mountains (Switzerland and France), Geol. Croatica, 56, 1–18, 2003.

Strasser, A., Pittet, B., Hillgärtner, H., Pasquier, J.-B.: Depositional sequences in shallow carbonate dominated sedimentary systems: concepts for a high-resolution analysis, Sed. Geol., 128, 201–221, https://doi.org/10.1016/S0037-0738(99)00070-6, 1999.

Strasser, A., Hillgärtner, H., Hug, W., and Pittet, B.: Third-order depositional sequences reflecting Milankovitch cyclicity, Terra Nova, 12, 303–311, https://doi.org/10.1046/j.1365-3121.2000.00315.x, 2000.

Strasser, A., Védrine, S., and Stienne, N.: Rate and synchronicity of environmental changes on a shallow carbonate platform (Late Oxfordian, Swiss Jura Mountains), Sedimentology, 59, 185–211, https://doi.org/10.1111/j.1365-3091.2011.01236.x, 2012.

Strasser, A., Pittet, B., and Hug, W.: Palaeogeography of a shallow carbonate platform: The case of the Middle to Late Oxfordian in the Swiss Jura Mountains, J. Palaeogeo., 4, 251–268, https://doi.org/10.1016/j.jop.2015.08.005, 2015.

Thiry, M.: Palaeoclimatic interpretation of clay minerals in marine deposits: an outlook from the continental origin, Earth-Sci. Rev., 49, 201–221, https://doi.org/10.1016/S0012-8252(99)00054-9, 2000.

Valero, L., Garcés, M., Cabrera, L., Costa, E., and Sáez, A.: 20 Myr of eccentricity paced lacustrine cycles in the Cenozoic Ebro Basin, Earth Planet. Sci. Lett., 408, 183–193, https://doi.org/10.1016/j.epsl.2014.10.007, 2014.

Védrine, S.: High-frequency palaeoenvironmental changes in mixed carbonate–siliciclastic sedimentary systems (Late Oxfordian, Switzerland, France, and southern Germany), Ph.D. thesis, GeoFocus, 19, Univ. Fribourg, Switzerland, 216 pp., 2007.

Védrine, S. and Strasser, A.: High-frequency palaeoenvironmental changes on a shallow carbonate platform during a marine transgression (Late Oxfordian, Swiss Jura Mountains), Swiss J. Geosci., 102, 247–270, https://doi.org/10.1007/s00015-009-1326-0, 2009.

Védrine, S., Strasser, A., and Hug, W.: Oncoid growth and distribution controlled by sea-level fluctuations and climate (Late Oxfordian, Swiss Jura Mountains), Facies, 53, 535–552, https://doi.org/10.1007/s10347-007-0114-4, 2007.

Wallmann, K., Schneider, B., and Sarnthein, M.: Effects of eustatic sea-level change, ocean dynamics, and nutrient utilization on atmospheric pCO_2 and seawater composition over the last 130000 years: a model study, Clim. Past, 12, 339–375, https://doi.org/10.5194/cp-12-339-2016, 2016.

Weissert, H. and Mohr, H.: Late Jurassic climate and its impact on carbon cycling, Palaeogeo. Palaeoclim., Palaeoecol., 122, 27–43, https://doi.org/10.1016/0031-0182(95)00088-7, 1996.

Wendler, J. E. and Wendler, I.: What drove sea-level fluctuations during the mid-Cretaceous greenhouse climate? Palaeogeo. Palaeoclim., Palaeoeco., 441, 412–419, https://doi.org/10.1016/j.palaeo.2015.08.029, 2016.

Wendler, J. E., Wendler, I., Vogt, C., and Kuss, J.: Link between cyclic eustatic sea-level change and continental weathering: evidence for aquifer-eustasy in the Cretaceous, Palaeogeo. Palaeoclim., Palaeoeco., 441, 430–437, https://doi.org/10.1016/j.palaeo.2015.08.014, 2016.

Wildi, W., Funk, H., Loup, B., Amato, E., and Huggenberger, P.: Mesozoic subsidence history of the European marginal shelves of the Alpine Tethys (Helvetic realm, Swiss Plateau and Jura), Eclogae Geol. Helv., 82, 817–840, 1989.

Wood, R.: Reef Evolution, Oxford Univ. Press, 432 pp., ISBN 9780198577843, 1999.

Zühlke, R.: Integrated cyclostratigraphy of a model Mesozoic carbonate platform – the Latemar (Middle Triassic, Italy), SEPM Spec. Publ., 81, 183–211, 2004.